

Dilepton bremsstrahlung from pion-pion scattering in a relativistic OBE model

H. C. Eggers

*Department of Physics, McGill University, Montréal, Québec H3A 2T8, Canada
and Institut für Hochenergiephysik der Österreichischen Akademie der Wissenschaften,
Nikolsdorfgasse 18, A-1050 Vienna, Austria*

R. Tabti, C. Gale

Department of Physics, McGill University, Montréal, Québec H3A 2T8, Canada

K. Haglin

*National Superconducting Cyclotron Laboratory, Michigan State University
East Lansing, MI 48824-1321, USA*

(October 1995)

Abstract

We have made a detailed and quantitative study of dilepton production via bremsstrahlung of a virtual photon during pion-pion collisions. Most calculations of electromagnetic radiation from strong interaction processes rely on the soft photon approximation (SPA). The conditions underlying this approximation are generally violated when dilepton spectra are calculated in terms of their invariant mass, so that an approach going beyond the SPA becomes necessary. Superseding previous derivations, we derive an exact formula for the bremsstrahlung cross section. The resulting formulation is compared to various forms based on the SPA, the two-particle phase space approximation and Rückl's formula using a relativistic One Boson Exchange (OBE) model. Within the OBE approach, we show that approximations to the bremsstrahlung dilepton cross sections often differ greatly from the exact result; discrepancies become greater both with rising temperature and with invariant mass. Integrated dilepton production rates are overestimated by Rückl-based approximations by factors 1.5–8.0. The largest discrepancies occur for the reaction $\pi^+\pi^+ \rightarrow \pi^+\pi^+\ell^+\ell^-$, where such approximations overestimate the exact rate by factors ranging from 2 to 30 for invariant masses between 10 and 500 MeV. Our findings, combined with recent estimates of the Landau-Pomeranchuk effect, indicate that bremsstrahlung dileptons rates in ultrarelativistic heavy ion collisions should be even more suppressed than

had been thought before.

13.40.-f, 25.75.-q, 13.75.Lb, 25.80.Ek

I. INTRODUCTION

Dileptons produced in heavy ion collisions interact only electromagnetically with their hadronic surroundings. Especially the early phases of such collisions, when dilepton production rates are largest, can therefore be explored with lepton pairs. Some of the initial ideas on photon [1] and dilepton [2] [3] emission have met with considerable interest, and this area has now expanded into a major component of research in ultrarelativistic heavy ion collisions [4]. On the experimental side, dilepton experiments for hadronic collisions [5]– [8] have been complemented only recently by nucleus-nucleus experiments at very high energies [9]– [12]. Since the spectrum of lepton pairs and of real photons has been proposed as a signature of the quark-gluon plasma [4], it is imperative quantitatively to understand the emission mechanisms from the confined sector of QCD, which in this sense constitutes the background.

Guided by theoretical estimates, we can roughly divide the lepton pair production cross section, expressed in terms of its invariant mass M , into a number of distinct regions. For $M > m_{J/\psi}$, the Drell-Yan contribution dominates, while pairs arising from the semileptonic decay of $D\bar{D}$ are also important [13]. For lepton pair invariant masses around the light vector meson masses (ρ , ω , and ϕ), two-body [14] and three-body [15] reactions dominate. The latter processes also extend their influence to the region $m_\phi < M < m_{J/\psi}$, where the quark-gluon plasma may become visible for sufficiently high initial temperatures [16]. In this paper, we concentrate on the regions of low invariant masses, the so-called “soft” limit $M \leq 300$ MeV. There, production via bremsstrahlung is expected to play an important role and many authors have recently concerned themselves with such reactions [17]– [28].

Since particle production plays an important role in ultrarelativistic heavy ion collisions, we consider only events that arise from microscopic meson-meson dynamics. In high energy heavy ion experiments, the meson to baryon ratio is such that the absence of baryons in our treatment is not expected to constitute a major hurdle to phenomenology. More specifically, we restrict our studies to those of pion-pion bremsstrahlung.

The production of photons or dileptons necessarily involves 3- or 4-particle final states. Except for special cases such as cross sections at fixed \mathbf{q} [29], such final states have universally been handled under some approximation. It is our goal in this paper to go beyond these by presenting an essentially exact formulation for the $\pi\pi \rightarrow \pi\pi\ell^+\ell^-$ cross section (as a function of dilepton invariant mass) and, in the process, to test how far these approximations may be trusted. In order to achieve these goals, we formulate the pion-pion interaction in terms of a relativistic One Boson Exchange model (OBE).

Note that we do not attempt to compare directly to experimental data because the main point at issue is a comparison of theoretical approaches to bremsstrahlung. To do justice to small- M data would require spacetime integration over the fireball region as well as inclusion of Dalitz decays and the Landau-Pomeranchuk effect, a substantial task which will be postponed to future work.

Our paper is organized as follows: in the next section, we discuss the set of approximations known under the collective banner of the Soft Photon Approximation (SPA). Next, we derive exact formulae for the bremsstrahlung generation of lepton pairs. Section IV is devoted to technical issues having to do with phase space; Sections V and VI then derive cross sections based respectively on various SPA variants and the exact formulation. Our

OBE model is presented in Section VII; finally, Section VIII contains our numerical results in the form of cross sections $d\sigma(s)/dM$ and rates $dN/d^4x dM$ and a discussion on the issues raised.

II. THE SOFT PHOTON APPROXIMATION

The Soft Photon Approximation (SPA) has been widely used in calculating bremsstrahlung dilepton spectra. It is based on the early realization [30] that the cross section for production of low-energy real photons is dominated by the corresponding hadronic amplitude. In practice, this means neglecting the photon momentum in the hadronic matrix element as well as all photon emission from vertices and internal lines (see Section II B).

A. Limitations

In order for the SPA to be a valid approximation, two conditions [31] must be met:

1. The photon energy must be much smaller than the energy of any one of the hadrons participating in the scattering,

$$q_0/E \ll 1, \quad (1)$$

2. the process of radiating the photon must be separable from the hadronic interaction process, i.e. the hadronic and electromagnetic time and distance scales must be sufficiently different to permit separate treatment. The range of the hadron-hadron interaction is given roughly by $b = m_Y^{-1}$, the inverse mass of the exchange boson, while the distance the hadron may propagate with off-shell energy $\Delta E = q_0$ before emitting the photon is about $\Delta x = v/\Delta E = |\mathbf{p}|/E q_0$. The SPA is valid only when $\Delta x/b \gg 1$, or

$$q_0 \ll m_Y |\mathbf{p}|/E. \quad (2)$$

Implicit in these equations is, of course, a specific Lorentz frame with respect to which the energies are measured. For the special case where two hadrons of equal mass m collide, these conditions can be re-written in their cms frame as

$$q_0^* \ll \sqrt{s}/2, \quad (3)$$

$$q_0^* \ll m_Y \sqrt{1 - 4m^2/s}. \quad (4)$$

In a simple bremsstrahlung experiment, these limits are easily satisfied by selecting only photons or dileptons of low energy in the laboratory frame. An early dilepton paper by Rückl, for example [32], calculated spectra for $\sqrt{s} = 27$ and 53 GeV while restricting transverse momentum to below 500 MeV.

In the complex multiparticle systems formed in the course of nucleus-nucleus collisions, however, the situation is more complicated: There are many binary collisions, and their

respective cms frames do not generally coincide either with one another or with the overall nucleus-nucleus cms frame. A photon that is soft in a particular hadron-hadron cms therefore does not have to be soft in the laboratory and vice versa. (This fact has to be taken into account when addressing issues related to the spectrum of real photons [33].)

In a situation where there are many cms frames, it therefore becomes necessary to look at relativistically invariant quantities. For lepton pairs, the extra degree of freedom provided by a non-vanishing invariant mass is a suitable variable of choice. Looking at invariant masses means, however, that q_0 is no longer fixed but must vary over its full kinematic range, which for our example of colliding equal-mass hadrons is given by (see Section V)

$$M \leq q_0 \leq \frac{s - 4m^2 + M^2}{2\sqrt{s}}. \quad (5)$$

Once the upper kinematic limit for q_0 approaches or exceeds the bounds set by either Eq. (3) or (4), the Soft Photon Approximation clearly fails.

In Figure 1, we show the three functions (3) and (4) and (5) for the case $m = m_\pi = 140$ MeV, $m_Y = m_\sigma \simeq 500$ MeV and dilepton invariant masses $M = 10$ and 300 MeV. It is immediately clear that the assumptions underlying the SPA are not fulfilled even for small M : the kinematic range accessible to q_0 is never much smaller than the limits set by the SPA. The situation becomes even worse for larger M .

Closely related to the above is a common misconception that the SPA must necessarily be valid for small invariant masses. The confusion stems from the fact that, because

$$M^2 = q_0^2 - \mathbf{q}^2, \quad (6)$$

a small value for q_0 necessarily implies small M . However, the reverse is not true: both q_0 and \mathbf{q} can be large even while adding up to small M . An extreme counterexample is of course a hard real photon with zero invariant mass but large energy. One cannot, therefore, a priori expect SPA calculations to coincide with full hadronic calculations even when M is small. Section VIII provides examples of such deviations; see especially the ratios between approximations and the exact calculation in Figures 12 and 13 which do not approach unity for small M . This point has been emphasized before [19].

We are therefore led to conclude that the SPA does not generally apply to rates or cross sections measured in terms of the dilepton invariant mass. Correspondingly, doubt must be cast on the validity of the SPA in calculations pertaining to such measurements.

That said, one may still ask *by how much* SPA-based calculations differ from the more complicated true situation: is it a matter of a few percent, or orders of magnitude? Full calculations such as presented in Section VII below are cumbersome and time-consuming, and it is therefore of value to understand quantitatively to what percentage the SPA approximation can be trusted. It is this *quantitative* question that we attempt to cast some light on by making a model calculation capable both of “true” answers and an SPA approximation.

Clearly, a single model calculation such as presented below cannot answer this quantitative question exhaustively. Nevertheless, its results provide at least an indicator of the reliability of the SPA: If, within our simple OBE, dileptons can or cannot reasonably be described within the SPA, it is possible or even likely that the same or similar conclusions would emerge from other models.

B. The SPA as series of approximations

Rather than being just a single step, the soft photon approximation as implemented in a practical context can consist of a number of stages. Starting with the most fundamental, these are:

- (A) The virtual photon producing the lepton pair is emitted only by external legs of the hadronic reaction; emission from internal parts of the hadronic reaction is neglected because the radiation from internal lines forms a sub-leading contribution [31].
- (B) The dependence of the hadronic matrix element \mathcal{M}_h on the photon momentum q is neglected.
- (C) The photon momentum q is neglected in the phase space delta functions.

In addition, we shall be considering in this paper the effect of

- (D) approximating the virtual photon current by the real photon current, $(J^\mu = \sum(2p_i^\mu \pm q)/(2p_i \cdot q \pm M^2) \rightarrow \sum p_i^\mu/(p_i \cdot q)$; see Eqs. (15) and (16)).

(A) and (B) have formed the basis for most bremsstrahlung dilepton calculations as they are hard to avoid. The restriction of phase space (C), on the other hand, can be circumvented fairly easily by inserting later a phase space correction factor (Section V A) or by avoiding (C) altogether using Eqs. (25), (36) and Sections IV and VI.

The change from virtual to real photon currents in step (D) is not directly dependent on (C) and can be implemented either jointly or separately. We shall be investigating both alternatives and determining their impact on the overall dilepton rate. In Section III B and Section VII and beyond, we shall refrain from using even the basic assumptions (A) and (B) and calculate exact cross sections and rates within the same lagrangian.

III. BREMSSTRAHLUNG CROSS SECTION

We wish to find the cross section for a dilepton pair $\ell^+\ell^-$ emitted in the semi-elastic scattering of two pions a and b into 1 and 2,

$$\pi_a + \pi_b \rightarrow \pi_1 + \pi_2 + \ell^+ + \ell^- . \quad (7)$$

The lepton pair forms via a virtual photon γ^* with four-momentum q^μ and mass $q^2 = M^2$ emitted from either the central blob or external legs of the hadronic reaction

$$\pi_a + \pi_b \rightarrow \pi_1 + \pi_2 . \quad (8)$$

The leading contribution will come from photon emission from external pion legs. First, we follow Lichard [26] in a leading-terms derivation but place more emphasis on the role of phase space; the full formalism supplanting the leading-terms derivation is presented in Section III B.

A. Bremsstrahlung from external legs

Four diagrams contribute to the leading-term cross section, one of which is shown in Figure 2. In the notation of Figure 2, the total matrix element can be written as products of purely hadronic reactions \mathcal{M}_h with currents J_i^μ and a leptonic part L_μ [34],

$$\begin{aligned} \mathcal{M}_{\ell^+\ell^-} = e [& J_a^\mu \mathcal{M}_h(p_a - q, p_b, p_1, p_2) + J_b^\mu \mathcal{M}_h(p_a, p_b - q, p_1, p_2), \\ & + J_1^\mu \mathcal{M}_h(p_a, p_b, p_1 + q, p_2) + J_2^\mu \mathcal{M}_h(p_a, p_b, p_1, p_2 + q)] L_\mu, \end{aligned} \quad (9)$$

where

$$L_\mu = \frac{e}{M^2} \bar{u}(p_-) \gamma_\mu v(p_+), \quad (10)$$

and, in slightly condensed notation, the terms of the pionic current are

$$J_{a,b}^\mu = \frac{-Q_{a,b}(2p_{a,b} - q)^\mu}{2p_{a,b} \cdot q - M^2}, \quad (11)$$

$$J_{1,2}^\mu = \frac{Q_{1,2}(2p_{1,2} + q)^\mu}{2p_{1,2} \cdot q + M^2}, \quad (12)$$

with Q_i the charge of pion i in units of the proton charge. Note that J_i^μ contains the propagator for the off-shell pion. Making approximation (B), one now neglects the dependence on q of the four hadronic matrix elements; for example

$$\mathcal{M}_h(p_a - q, p_b, p_1, p_2) \sim \mathcal{M}_h(p_a, p_b, p_1, p_2), \quad (13)$$

permitting the usual factorization of $\mathcal{M}_{\ell^+\ell^-}$ into a purely hadronic matrix element and a photon-plus-lepton part:

$$\mathcal{M}_{\ell^+\ell^-} \simeq e \mathcal{M}_h(p_a, p_b, p_1, p_2) J^\mu(p_a, p_b, p_1, p_2, q) L_\mu(p_+, p_-), \quad (14)$$

where now the virtual-photon current

$$J^\mu = \sum_{i=1,2} Q_i \frac{(2p_i + q)^\mu}{2p_i \cdot q + M^2} - \sum_{i=a,b} Q_i \frac{(2p_i - q)^\mu}{2p_i \cdot q - M^2} \quad (15)$$

contains the sum over the four diagrams. Since approximations (A) and (B) are valid only for photons of small q and by implication for small M , the extra terms in numerator and denominator are usually neglected (in what we called approximation (D)) to form the real-photon current

$$I^\mu = \sum_{i=1,2} Q_i \frac{p_i^\mu}{p_i \cdot q} - \sum_{i=a,b} Q_i \frac{p_i^\mu}{p_i \cdot q}. \quad (16)$$

Squaring the total matrix element and summing over lepton polarizations (s_+, s_-) yields, using either current [26],

$$\begin{aligned}
\sum_{s_+, s_-} |\mathcal{M}_{\ell^+ \ell^-}|^2 &= 4\pi\alpha |\mathcal{M}_h(p_a, p_b, p_1, p_2)|^2 J^\mu J^\nu L_{\mu\nu} \\
&= |\mathcal{M}_h|^2 \frac{32\pi^2 \alpha^2}{M^2} \left[-J \cdot J - \frac{(l \cdot J)^2}{M^2} \right], \tag{17}
\end{aligned}$$

where $l = p_+ - p_-$ and the leptonic tensor is

$$L_{\mu\nu} = \sum_{s_+, s_-} L_\mu L_\nu^* = \frac{8\pi\alpha}{M^4} (q_\mu q_\nu - l_\mu l_\nu - M^2 g_{\mu\nu}). \tag{18}$$

At this point, q is still defined only as the sum of lepton momenta ($p_+ + p_-$).

With $F = 4[(p_a \cdot p_b)^2 - m_a^2 m_b^2]^{1/2}$ the incoming flux, the unpolarized cross section is an integral over phase space of *four* outgoing particles,

$$d\sigma_{hh\ell^+\ell^-} = \sum_{s_+, s_-} |\mathcal{M}_{\ell^+ \ell^-}|^2 \frac{dR_4}{(2\pi)^8 F}, \tag{19}$$

$$dR_4 \equiv \delta^4(p_a + p_b - p_1 - p_2 - p_+ - p_-) d\tau_1 d\tau_2 d\tau_+ d\tau_- \tag{20}$$

where we write $d\tau_i = d^3\mathbf{p}_i/2E_i$ for short. This can be reduced to a *three*-particle phase space integral by changing variables and integrating over redundant degrees of freedom in the dilepton cms,

$$d\tau_+ d\tau_- = \frac{1}{8} \sqrt{1 - \frac{4\mu^2}{M^2}} dM^2 d\tau_q d\Omega_+, \tag{21}$$

where the positron solid angle Ω_+ must be kept due to the $(l \cdot J)$ term, and μ is the lepton mass. The dependence of $(l \cdot J)$ on Ω_+ is integrated out,

$$\int \left[-J^2 - \frac{(l \cdot J)^2}{M^2} \right] d\Omega_+ = \frac{8\pi}{3} \left(1 + \frac{2\mu^2}{M^2} \right) (-J^2), \tag{22}$$

so that, using Eqs. 17–22, we can express the total cross section in terms of a leptonic factor κ and a “hadronic plus virtual photon” cross section $d\sigma_{hh\gamma^*}$,

$$d\sigma_{hh\ell^+\ell^-} = \kappa(\mu^2, M^2) d\sigma_{hh\gamma^*}, \tag{23}$$

with

$$\kappa \equiv M^2 \tau(M^2) \equiv \frac{\alpha}{3\pi} \left(1 + \frac{2\mu^2}{M^2} \right) \sqrt{1 - \frac{4\mu^2}{M^2}}, \tag{24}$$

and where

$$d\sigma_{hh\gamma^*} = 4\pi\alpha \frac{dM^2}{M^2} (-J^2) |\mathcal{M}_h|^2 \frac{dR_3}{(2\pi)^5 F} \tag{25}$$

is a function of *three*-particle phase space

$$dR_3 = \delta^4(p_a + p_b - p_1 - p_2 - q) d\tau_1 d\tau_2 d\tau_q. \tag{26}$$

With the understanding that its derivation is valid under approximations (A) and (B) only, Eq. (23) is exact and makes no assumptions with respect to phase space. In particular, we note that q is still contained in the delta function constraining the phase space in Eq. (26). Next, we shall show that Eq. (23) is valid even when approximations (A) and (B) are not made but that $d\sigma_{hh\gamma^*}$ takes on a form different from Eq. (25).

B. Emission from all diagrams

When calculating dilepton cross sections for all possible diagrams, including internal emission of photons, it is no longer possible to factorize the matrix element into a hadronic part and a current as in Eq. (9). Instead, we consider, for a given pion-pion reaction, the full matrix element

$$\mathcal{M}(\pi\pi \rightarrow \pi\pi \ell^+ \ell^-) = \mathcal{M}^\mu L_\mu = \sum_m \mathcal{M}_m^\mu L_\mu, \quad (27)$$

where m runs over all contributing diagrams. The sum of diagrams is gauge invariant,

$$q_\mu \mathcal{M}^\mu = \sum_m q_\mu \mathcal{M}_m^\mu = 0, \quad (28)$$

but not necessarily the individual terms. Unlike in the previous sections \mathcal{M}^μ contains, besides the hadronic interaction, the photon vertex and where applicable the external pion propagator, both of which were previously part of the current.

Starting again with the cross section in four-phase space (19) and transforming from $d\tau_+ d\tau_-$ to $d\tau_q dM^2 d\Omega_+$ using Eq. (21), the unpolarized dilepton cross section is

$$d\sigma_{hh\ell^+\ell^-} = \sqrt{1 - \frac{4\mu^2}{M^2}} \frac{dM^2 d\tau_1 d\tau_2 d\tau_q \delta(\dots)}{8(2\pi)^8 F} \int d\Omega_+ \sum_{s^+ s^-} |\mathcal{M}_{\ell^+\ell^-}|^2. \quad (29)$$

Squaring and summing over lepton polarizations, we obtain in analogy to Eq. (17)

$$\sum_{s^+ s^-} |\mathcal{M}^\mu L_\mu|^2 = \sum_{m,n} \mathcal{M}_m^\mu \mathcal{M}_n^{*\nu} L_{\mu\nu}, \quad (30)$$

where as before $L_{\mu\nu} = 8\pi\alpha(q_\mu q_\nu - l_\mu l_\nu - M^2 g_{\mu\nu})/M^4$. In the dilepton cms, $l_0 = 0$ and the second term in $L_{\mu\nu}$ integrates to

$$\begin{aligned} \int d\Omega_+ l_\mu \mathcal{M}_m^\mu l_\nu \mathcal{M}_n^{*\nu} &= 4 \int d\Omega_+ (\mathbf{p}_+ \cdot \mathcal{M}_m) (\mathbf{p}_+ \cdot \mathcal{M}_n^*), \\ &= \frac{4\pi}{3} (M^2 - 4\mu^2) \mathcal{M}_m \cdot \mathcal{M}_n^*. \end{aligned} \quad (31)$$

Since $\mathbf{q} = 0$ in this frame, $\mathcal{M}_m^0 = q_\mu \mathcal{M}_m^\mu / q_0$ and hence in the dilepton cms

$$\mathcal{M}_m \cdot \mathcal{M}_n^* = q_0^{-2} (q_\mu \mathcal{M}_m^\mu) (q_\nu \mathcal{M}_n^{*\nu}) - \mathcal{M}_m \cdot \mathcal{M}_n^*, \quad (32)$$

so, using gauge invariance (28),

$$\sum_{mn} \mathcal{M}_m \cdot \mathcal{M}_n^* (\text{cms}) = - \sum_{mn} \mathcal{M}_m \cdot \mathcal{M}_n^*. \quad (33)$$

Hence

$$\int d\Omega_+ \sum_{s^+ s^-} |\mathcal{M}^\mu L_\mu|^2 = \frac{64\pi^2 \alpha}{3M^2} \left(1 + \frac{2\mu^2}{M^2}\right) \left(- \sum_{m,n} \mathcal{M}_m \cdot \mathcal{M}_n^*\right), \quad (34)$$

and the full cross section becomes

$$d\sigma_{hh\ell^+\ell^-} = \kappa(M^2)d\sigma_{hh\gamma^*}, \quad (35)$$

which is identical to Eq. (23), but with the virtual photon cross section reading

$$d\sigma_{hh\gamma^*} = \frac{dM^2}{M^2} \left(- \sum_{mn} \mathcal{M}_m \cdot \mathcal{M}_n^* \right) \frac{dR_3}{(2\pi)^5 F}. \quad (36)$$

Comparing to eq. (25), we have the correspondence $4\pi\alpha(-J^\mu J_\mu)|\mathcal{M}_h|^2 \leftrightarrow (-\sum_{mn} \mathcal{M}_m^\mu \mathcal{M}_{n\mu}^*)$.

Equations (35) and (36), together with use of the 3-phase space variables of Section IV provide a fully covariant formalism capable of exact treatment of both hadronic and electromagnetic sectors of a given model. Within the physical limitations implicit in a given model, it makes no further assumptions or approximations. In particular, none of the approximations listed in Section II B are needed.

C. Dilepton rates

In the context of nuclear collisions, one is interested more in overall dilepton rates than in fixed- s cross sections. Not attempting to account fully for either quantum statistical or flow effects here, we shall make the simplest assumption of a locally thermal Boltzmann gas of pions at a (local) temperature T . The rate of pair production of invariant mass M per unit of four-volume then is [3]

$$\frac{dN_{\ell^+\ell^-}^{\text{Boltz}}}{d^4x dM^2} = \frac{g_{ab}}{32\pi^4} \int ds \lambda(s, m_a^2, m_b^2) \frac{K_1(\sqrt{s}/T)}{(\sqrt{s}/T)} \frac{d\sigma_{hh\ell^+\ell^-}}{dM^2}, \quad (37)$$

where

$$\lambda(x, y, z) = (x - y - z)^2 - 4yz \quad (38)$$

is the basic three-particle kinematic function [35], which for equal masses ($m_a = m_b = m_1 = m_2$) has the more familiar form $\lambda(s, m^2, m^2) = s(s - 4m^2)$, and $g_{ab} = (2S_a + 1)(2S_b + 1)$ is the spin degeneracy factor which for pions is unity. K_1 is the modified Bessel function.

IV. THREE-PARTICLE PHASE SPACE

To complete our preparatory work, we summarize the treatment of three-particle phase space in terms of relativistic invariants. The relations of this section will be useful first in 3-phase space integration of the currents (15) and (16) and later in the exact treatment of bremsstrahlung dilepton production.

Three-particle phase space has been studied extensively and we here merely outline the procedure; for details see Ref. [35]. As shown in Figure 3, the kinematics for a reaction

$$a + b \longrightarrow 1 + 2 + 3 \quad (39)$$

can be described in terms of the five invariants $s = (p_a + p_b)^2$, $t_1 = (p_1 - p_a)^2$, $s_1 = (p_1 + p_2)^2$, $s_2 = (p_2 + p_3)^2$, and $t_2 = (p_b - p_3)^2$. For our purposes, we shall be using p_3 and q interchangeably as referring to the virtual photon, i.e. $E_3 \equiv q_0$ and $q^2 = m_3^2 \equiv M^2$. The other momenta refer, as usual, to the incoming and outgoing hadrons. Inverting, one gets

$$\begin{aligned}
2p_a \cdot p_b &= s - m_a^2 - m_b^2, \\
2p_a \cdot p_1 &= m_a^2 + m_1^2 - t_1, \\
2p_a \cdot p_2 &= s_1 + t_1 - t_2 - m_1^2, \\
2p_b \cdot p_1 &= s - s_2 + t_1 - m_a^2, \\
2p_b \cdot p_2 &= s_2 + t_2 - t_1 - M^2, \\
2p_1 \cdot p_2 &= s_1 - m_1^2 - m_2^2, \\
2p_a \cdot q &= s - s_1 + t_2 - m_b^2, \\
2p_b \cdot q &= m_b^2 + M^2 - t_2, \\
2p_1 \cdot q &= s - s_1 - s_2 + m_2^2, \\
2p_2 \cdot q &= s_2 - m_2^2 - M^2.
\end{aligned} \tag{40}$$

The corresponding phase space integral is

$$dR_3(s) = \frac{\pi}{4\lambda^{1/2}(s, m_a^2, m_b^2)} \int \frac{dt_1 ds_2 ds_1 dt_2}{\sqrt{B}}, \tag{41}$$

where the weighting is given in terms of the Cayley determinant

$$B = \begin{vmatrix} 0 & 1 & 1 & 1 & 1 & 1 \\ 1 & 0 & m_2^2 & s_2 & t_1 & m_1^2 \\ 1 & m_2^2 & 0 & M^2 & t_2 & s_1 \\ 1 & s_2 & M^2 & 0 & m_b^2 & s \\ 1 & t_1 & t_2 & m_b^2 & 0 & m_a^2 \\ 1 & m_1^2 & s_1 & s & m_a^2 & 0 \end{vmatrix}. \tag{42}$$

The Cayley determinant is quadratic in any of its arguments; specifically, we use the form

$$B = \lambda(s, s_2, m_1^2) (t_2^+ - t_2)(t_2 - t_2^-), \tag{43}$$

where the kinematic limits on t_2 are given by

$$\begin{aligned}
t_2^\pm &= m_b^2 + M^2 - \frac{1}{\lambda(s, s_2, m_1^2)} \begin{vmatrix} 2s & s+s_2-m_1^2 & s-s_1+M^2 \\ s+s_2-m_1^2 & 2s_2 & s_2-m_2^2+M^2 \\ s-m_a^2+m_b^2 & s_2-t_1+m_b^2 & 0 \end{vmatrix} \\
&\pm \frac{2}{\lambda(s, s_2, m_1^2)} [G(s, t_1, s_2, m_a^2, m_b^2, m_1^2)G(s_1, s_2, s, m_2^2, m_1^2, M^2)]^{1/2},
\end{aligned} \tag{44}$$

written in terms of yet another determinant and the basic four-particle kinematic function

$$G(x, y, z, u, v, w) \equiv - \left(\frac{1}{2}\right) \begin{vmatrix} 0 & 1 & 1 & 1 & 1 \\ 1 & 0 & v & x & z \\ 1 & v & 0 & u & y \\ 1 & x & u & 0 & w \\ 1 & z & y & w & 0 \end{vmatrix}. \tag{45}$$

The kinematic limits on s_1 are

$$s_1^\pm = s + M^2 - \frac{1}{2s_2}(s + s_2 - m_1^2)(s_2 + M^2 - m_2^2) \pm \frac{1}{2s_2}\lambda^{1/2}(s, s_2, m_1^2) \lambda^{1/2}(s_2, m_2^2, M^2). \quad (46)$$

The limits on s_2 and t_1 are given by the Chew-Low plot: for values of t_1 bounded by

$$t_1^\pm = m_a^2 + m_1^2 - \frac{1}{2s}[s + m_a^2 - m_b^2][s + m_1^2 - (m_2 + M)^2] \pm \frac{1}{2s}\lambda^{1/2}(s, m_a^2, m_b^2) \lambda^{1/2}(s, (m_2 + M)^2, m_1^2), \quad (47)$$

the limits on s_2 are

$$s_2^+ = s + m_1^2 - \frac{1}{2m_a^2}[s + m_a^2 - m_b^2][m_a^2 + m_1^2 - t_1] + \frac{1}{2m_a^2}\lambda^{1/2}(s, m_a^2, m_b^2) \lambda^{1/2}(t_1, m_a^2, m_1^2), \quad (48)$$

$$s_2^- = (m_2 + M)^2. \quad (49)$$

Although not directly relevant for pions, we include for completeness the case where the hadronic masses m_a and m_1 are unequal. In this case, t_1 may become larger than t_1^+ given above, and the corresponding additional phase space is delimited by

$$t_1^+ \leq t_1 \leq (m_a - m_1)^2 \quad (50)$$

and for this additional domain, s_2 is limited by s_2^+ of Eq. (48) and the corresponding lower branch, given by a minus sign before the λ -factors. Clearly, t_1 resembles the 2-phase space invariant t , but they are distinct quantities due to the presence of the additional momentum q .

Integration over pure phase space yields

$$\frac{dR_3}{dt_1}(s, t_1) = \int_{s_2^-}^{s_2^+} ds_2 \frac{\lambda^{1/2}(s_2, m_2^2, M^2)}{s_2} = F(s_2^+) - F(s_2^-), \quad (51)$$

where

$$F(s_2) = l_2 - (m_2^2 + M^2) \ln(s_2 + l_2 - m_2^2 - M^2) - (m_2^2 - M^2) \ln(s_2 + l_2 + m_2^2 - M^2) - (M^2 - m_2^2) \ln(s_2 + l_2 - m_2^2 + M^2), \quad (52)$$

and we have written $l_2 = \lambda^{1/2}(s_2, m_2^2, M^2)$ for short. This yields identical results to the pure phase space formula (66) below, as it should. We note in passing that the ratio of the kinematic domains of (3-space) t_1 to (2-space) t is exactly the phase space reduction factor found in (69) below.

V. ANGLE-AVERAGED-CURRENT APPROXIMATIONS

All the elements for our calculation are now in place. In this section, we look at three approximations of increasing sophistication. We proceed first to find explicit expressions for the pion-pion-photon cross section $d\sigma_{hh\gamma^*}$ of Eq. (25) based on the factorization into a current and hadronic matrix element of Section III A. These approximations are based on an angular average of $(-J^2)$ in the ab center-of-momentum frame. Using three-space invariants, we integrate the current covariantly in Section V C.

A. The Ruckl formula

In 1976, Ruckl proposed [32] that the dilepton cross section be written in terms of the *real photon* cross section:

$$E_+ E_- \frac{d\sigma_{hh\ell^+\ell^-}}{d^3\mathbf{p}_+ d^3\mathbf{p}_-} = \frac{\alpha}{2\pi^2 M^2} q_0 \frac{d\sigma_{hh\gamma}}{d^3\mathbf{q}}. \quad (53)$$

This ansatz, now in common use, was utilized by Haglin et al. [22] and others previously [17,18,21,34] to derive dilepton production rates. In our notation, the Ruckl formula reads

$$d\sigma_{hh\ell^+\ell^-} = \frac{\alpha}{\pi^2 M^2} \frac{d\tau_+ d\tau_-}{d\tau_q} d\sigma_{hh\gamma}, \quad (54)$$

which becomes, using the formulas of the previous section, and approximating $\int d\Omega_+ = 4\pi$ and $\kappa \simeq \alpha/3\pi$,

$$d\sigma_{hh\ell^+\ell^-} = \frac{3}{2} \kappa d\sigma_{hh\gamma} \frac{dM^2}{M^2}. \quad (55)$$

The real-photon cross section $d\sigma_{hh\gamma}$ can be written down immediately from the virtual-photon cross section $d\sigma_{hh\gamma^*}$ of (25),

$$d\sigma_{hh\gamma} = 4\pi\alpha (-J^2) |\mathcal{M}_h|^2 \frac{dR_3}{(2\pi)^5 F}. \quad (56)$$

Neglecting q in the delta function of dR_3 , the 3-phase space integral of Eq. (26) factorizes into the usual 2-phase space and the \mathbf{q} -integration

$$dR_3 \simeq dR_2 d\tau_q, \quad (57)$$

with

$$dR_2 = \delta(p_a + p_b - p_1 - p_2) d\tau_1 d\tau_2, \quad (58)$$

leading all in all to

$$\frac{d\sigma_{hh\ell^+\ell^-}^{\text{Ruckl}}}{dM^2} = \frac{3}{2} \frac{\kappa}{M^2} \frac{\alpha}{\pi} \int d\sigma_{hh} (-J^2) \frac{d\tau_q}{2\pi}, \quad (59)$$

where

$$d\sigma_{hh} = |\mathcal{M}_h|^2 \frac{dR_2}{(2\pi)^2 F} \quad (60)$$

is the elastic hadronic cross section. Integrating $(-J^2)$ first with respect to the photon phase space with $d\tau_q = d\Omega_q |\mathbf{q}| dq_0/2$ leads to

$$\int (-J^2) \frac{d\tau_q}{2\pi} = \int_M^A dq_0 \sqrt{q_0^2 - M^2} \int \frac{d\Omega_q}{4\pi} (-J^2), \quad (61)$$

where $A = [s + M^2 - (m_1 + m_2)^2]/2\sqrt{s}$ is the upper kinematic boundary.

The angular average over $d\Omega_q$ was found by Haglin et al. for the real-photon current (16) in terms of velocities β_i in the $(\mathbf{p}_a + \mathbf{p}_b = 0)$ cms as [22]

$$\begin{aligned} \langle -I^2 \rangle &= \int \frac{d\Omega_q}{4\pi} (-I^2) \\ &= \frac{1}{q_0^2} \left[-(Q_a^2 + Q_b^2 + Q_1^2 + Q_2^2) - 2Q_a Q_b \mathcal{F}_{ab} - 2Q_1 Q_2 \mathcal{F}_{12} + 2 \sum_{i=a,b} \sum_{j=1,2} Q_i Q_j \mathcal{F}_{ij} \right], \quad (62) \end{aligned}$$

where

$$\mathcal{F}_{ij} \equiv \frac{(1 - \beta_i \cdot \beta_j)}{2D_{ij}} \left[\ln \left| \frac{\beta_i \cdot (\beta_j - \beta_i) - D_{ij}}{\beta_i \cdot (\beta_j - \beta_i) + D_{ij}} \right| + (i \leftrightarrow j) \right], \quad (63)$$

$$D_{ij} \equiv [(\beta_i - \beta_j)^2 - (\beta_i \times \beta_j)^2]^{1/2}. \quad (64)$$

To convert these angular averages into functions of 2-phase space invariants (s, t) , it is necessary to invoke approximation (C) restricting phase space: While $\mathbf{p}_a + \mathbf{p}_b = 0$ in the chosen frame, the presence of \mathbf{q} means that $\mathbf{p}_1 + \mathbf{p}_2 \neq 0$, i.e. β_1 and β_2 are not true cms velocities. Ignoring therefore \mathbf{q} at this point, the velocities and hence the angular averages can be written [22] in terms of s, t and q_0 ,

$$\begin{aligned} \langle -I^2 \rangle &= \frac{1}{q_0^2} \left[-(Q_a^2 + Q_b^2 + Q_1^2 + Q_2^2) \right. \\ &\quad - 2(Q_a Q_b + Q_1 Q_2) \frac{s - 2m^2}{\sqrt{s(s - 4m^2)}} \ln \left| \frac{s + \sqrt{s(s - 4m^2)}}{s - \sqrt{s(s - 4m^2)}} \right| \\ &\quad + 2(Q_a Q_1 + Q_b Q_2) \frac{2m^2 - t}{\sqrt{-t(s + u)}} \ln \left| \frac{\sqrt{-t(s + u)} - t}{\sqrt{-t(s + u)} + t} \right| \\ &\quad \left. + 2(Q_a Q_2 + Q_b Q_1) \frac{2m^2 - u}{\sqrt{-u(s + t)}} \ln \left| \frac{\sqrt{-u(s + t)} - u}{\sqrt{-u(s + t)} + u} \right| \right], \quad (65) \end{aligned}$$

with $u = 4m^2 - s - t$ as usual.

Having expediently eliminated q at two points, it is very important in this formulation to correct for phase space, i.e. to alleviate the effects of approximation (C). Pure phase space integration of dR_3 (including q in the delta function) yields exactly

$$\int dR_3 = \int d\tau_q \frac{\pi \lambda^{1/2}(s', m_a^2, m_b^2)}{2s'} \quad (66)$$

where

$$s' = s - 2q_0\sqrt{s} + M^2. \quad (67)$$

Integration over pure two-particle phase space, on the other hand, yields

$$\int dR_2 = \frac{\pi \lambda^{1/2}(s, m_1^2, m_2^2)}{2s}, \quad (68)$$

so $\int dR_2$, unconstrained by q , grossly overestimates $\int dR_3$, making it necessary to insert *a posteriori* the factor [36]

$$C(s, q_0) = \frac{s \lambda^{1/2}(s', m_a^2, m_b^2)}{s' \lambda^{1/2}(s, m_1^2, m_2^2)} \quad (69)$$

into the q_0 -integration (61). The ‘‘Rückl approximation’’ for dilepton production therefore reads, in its final form,

$$\frac{d\sigma_{hh\ell^+\ell^-}^{\text{Rückl}}(s)}{dM^2} = \frac{3}{2} \frac{\kappa}{M^2} \frac{\alpha}{\pi} \int d\sigma_{hh}(s, t) \int dq_0 |\mathbf{q}| C(s, q_0) \langle -I^2(s, t) \rangle; \quad (70)$$

this is the form used in Ref. [22].

B. Current formulae based on Lichard

Starting not from the Rückl formula but rather from Lichard’s improved formalism [26] of Section III A, the derivation proceeds along the same lines as the above. One finds correspondingly for the real-photon current

$$\frac{d\sigma_{hh\ell^+\ell^-}^{\text{L0}}(s)}{dM^2} = \frac{\kappa}{M^2} \frac{\alpha}{\pi} \int d\sigma_{hh}(s, t) \int dq_0 |\mathbf{q}| C(s, q_0) \langle -I^2(s, t) \rangle, \quad (71)$$

differing from the above by a constant factor 3/2 and the extra factors entering the exact version (24) of κ .

The corresponding virtual-photon current yields the third approximation within the angle-averaged current family,

$$\frac{d\sigma_{hh\ell^+\ell^-}^{\text{L1}}(s)}{dM^2} = \frac{\kappa}{M^2} \frac{\alpha}{\pi} \int d\sigma_{hh}(s, t) \int dq_0 |\mathbf{q}| C(s, q_0) \langle -J^2(s, t) \rangle. \quad (72)$$

where the angular average of (15) is

$$\begin{aligned} \langle -J^2 \rangle &= \int \frac{d\Omega_q}{4\pi} (-J^2) \\ &= - \frac{(Q_a^2 + Q_b^2)(4m^2 - M^2)}{q_0^2 s - \mathbf{q}^2 (s - 4m^2) - 2q_0\sqrt{s}M^2 + M^4} \end{aligned}$$

$$\begin{aligned}
& - \frac{(Q_1^2 + Q_2^2)(4m^2 - M^2)}{q_0^2 s - \mathbf{q}^2(s - 4m^2) + 2q_0\sqrt{s}M^2 + M^4} \\
& - \frac{Q_a Q_b(2s - 4m^2 - M^2)}{|\mathbf{q}|v_- \sqrt{s - 4m^2}} \ln \left| \frac{|\mathbf{q}|\sqrt{s - 4m^2} + q_0\sqrt{s} - M^2}{|\mathbf{q}|\sqrt{s - 4m^2} - q_0\sqrt{s} + M^2} \right| \\
& - \frac{Q_1 Q_2(2s - 4m^2 - M^2)}{|\mathbf{q}|v_+ \sqrt{s - 4m^2}} \ln \left| \frac{|\mathbf{q}|\sqrt{s - 4m^2} + q_0\sqrt{s} + M^2}{|\mathbf{q}|\sqrt{s - 4m^2} - q_0\sqrt{s} - M^2} \right| \\
& + \frac{(Q_a Q_1 + Q_b Q_2)(4m^2 - 2t + M^2)}{2\chi_t} \ln \left| \frac{(\mathbf{q}^2 t - \chi_t - M^2 v_-)(\mathbf{q}^2 t - \chi_t + M^2 v_+)}{(\mathbf{q}^2 t + \chi_t - M^2 v_-)(\mathbf{q}^2 t + \chi_t + M^2 v_+)} \right| \\
& + \frac{(Q_a Q_2 + Q_b Q_1)(4m^2 - 2u + M^2)}{2\chi_u} \ln \left| \frac{(\mathbf{q}^2 u - \chi_u - M^2 v_-)(\mathbf{q}^2 u - \chi_u + M^2 v_+)}{(\mathbf{q}^2 u + \chi_u - M^2 v_-)(\mathbf{q}^2 u + \chi_u + M^2 v_+)} \right|,
\end{aligned} \tag{73}$$

where

$$v_{\pm} \equiv q_0 \sqrt{s} \pm M^2, \tag{74}$$

$$\chi_t \equiv |\mathbf{q}| \sqrt{-t(sq_0^2 + u\mathbf{q}^2) - uM^4}, \tag{75}$$

$$\chi_u \equiv |\mathbf{q}| \sqrt{-u(sq_0^2 + t\mathbf{q}^2) - tM^4}. \tag{76}$$

Eq. (73) reduces to Eq. (65) for $M \rightarrow 0$. We shall be testing the effect of using the virtual over real-photon currents within the present approximation in Section VIII below. We note in passing that Eq. (73) would be preferable to Eq. (65) for very small hadron masses m , since then the latter is logarithmically sensitive to $1/m$ while the former is regulated by the dilepton invariant mass M .

C. Three-phase space current approximations

Three approximations were needed for the above angle-averaged current cross sections: the Rückl formula, converting cms velocities β_i to invariants s and t leading to Eqs. (62) and (63), and correcting for phase space using Eq. (69). At the cost of increased computing time, all three can be avoided by utilizing the formalism of three-particle phase space invariants.

Within 3-phase space, and writing the flux as $F = 2\lambda^{1/2}(s, m_a^2, m_b^2)$, the bremsstrahlung cross section of Eq. (25) becomes¹

$$\frac{d\sigma_{hh\ell^+\ell^-}}{dM^2}(s) \simeq \frac{4\pi\alpha}{(2\pi)^5 M^2} \frac{\kappa(M^2)\pi}{8\lambda(s, m_a^2, m_b^2)} \int dt_1 |\mathcal{M}_h(s, t_1)|^2 \int \frac{ds_2 ds_1 dt_2}{\sqrt{B}} \left[-J^2(s, t_1, s_2, s_1, t_2) \right]. \tag{77}$$

This differs from Eq. (72) in the way the current is treated: by an angular average plus q_0 -integration for the earlier, by full 3-phase space invariants in the present case. Note that \mathcal{M}_h is here a function of t_1 rather than t .

¹ Technically, it would in equation (77) be possible to restore q to \mathcal{M}_h and then to include it with $-J^2$ in the inner integral, but because of missing contact terms this procedure is not gauge invariant and shall not be pursued.

VI. EXACT CROSS SECTION

In all the above approximations, neglecting the dependence on q of the squared hadronic matrix element $|\mathcal{M}_h(p_a, p_b, p_1, p_2)|^2$ is unavoidable because this had been a precondition to factorizing into electromagnetic and hadronic parts in Eq. (9). There have been attempts to go beyond this on-shell matrix element approximation by expanding \mathcal{M}_h in q (see Refs. [26,27,34]), but this procedure involves successively more complicated derivatives without guaranteeing convergence.

Using 3-phase space invariants and the exact² expressions (36) for the pion-pion-photon cross section and (35) for the dilepton cross section, such expansions in q become superfluous. To calculate explicit dilepton cross sections, we merely insert from our favorite model for pion-pion scattering the complete set of matrix elements, and write the elements of the squared sum of (36) in terms of these invariants:

$$\mathcal{M}_m^\mu \mathcal{M}_{n\mu}^*(p_a, p_b, p_1, p_2, q) \longrightarrow \mathcal{M}_m^\mu \mathcal{M}_{n\mu}^*(s, t_1, s_2, s_1, t_2) \equiv T_{mn}. \quad (78)$$

This casting in terms of invariants means that q and all consequent off-shell effects in $|\mathcal{M}|^2$ are fully taken care of.³

Putting it all together, we obtain

$$\frac{d\sigma_{hh\ell^+\ell^-}^{\text{exact}}}{dM^2}(s) = \frac{4\pi\alpha}{(2\pi)^5 M^2} \frac{\kappa(M^2)\pi}{8\lambda(s, m_a^2, m_b^2)} \int \frac{dt_1 ds_2 ds_1 dt_2}{\sqrt{B}} \left[-\sum_{mn} T_{mn}(s, t_1, s_2, s_1, t_2) \right]. \quad (79)$$

While the cross sections may be exact, microscopic models for the pion-pion interaction are far from perfect. In the next section, we make use of a simple model to illustrate the present cross section and the approximations enumerated before. The main point of this section, however, is to stress that, apart from model-induced ailments, the exact treatment of any model for the reaction $\pi\pi \rightarrow \pi\pi\ell^+\ell^-$ is possible.

VII. GAUGE-INVARIANT OBE MODEL

To compare dilepton cross sections under the exact formula and various approximations introduced so far, we must make a model: little if any experimental data for the differential pion-pion-photon cross section is available. To this purpose, we return to a simple lagrangian with σ , ρ and $f(1270)$ exchange used previously [22] which, when t -integrated, successfully reproduced experimental data for elastic $\pi^+\pi^- \rightarrow \pi^+\pi^-$ scattering [37,38]:

$$\mathcal{L}_{\text{int}} = g_\sigma \sigma \partial_\mu \boldsymbol{\pi} \cdot \partial^\mu \boldsymbol{\pi} + g_\rho \rho^\mu \boldsymbol{\pi} \times \partial_\mu \boldsymbol{\pi} + g_f f_{\mu\nu} \partial^\mu \boldsymbol{\pi} \cdot \partial^\nu \boldsymbol{\pi}. \quad (80)$$

² To order α for the emission of real photons and to order α^2 for dilepton emission.

³ Matrix elements keeping their full dependence on q can be implemented within 2-phase space when only the *differential* cross section $d\sigma/d^3\mathbf{q} dM^2$ need be calculated; see e.g. Ref. [29]; for $d\sigma/dM^2$, this becomes impossible.

Here, we include the full momentum dependence of the f propagator which now reads [39,40]

$$i\mathcal{P}_{\alpha\beta\gamma\delta}(k) = \frac{-i f_{\alpha\beta\gamma\delta}(k)}{k^2 - m_f^2 + im_f\Gamma_f}, \quad (81)$$

$$\begin{aligned} f_{\alpha\beta\gamma\delta}(k) &= \frac{1}{2} (g_{\alpha\gamma}g_{\beta\delta} + g_{\alpha\delta}g_{\beta\gamma} - g_{\alpha\beta}g_{\gamma\delta}) \\ &\quad - \frac{1}{2} \left(g_{\alpha\gamma} \frac{k_\beta k_\delta}{m_f^2} + g_{\alpha\delta} \frac{k_\beta k_\gamma}{m_f^2} + g_{\beta\gamma} \frac{k_\alpha k_\delta}{m_f^2} + g_{\beta\delta} \frac{k_\alpha k_\gamma}{m_f^2} \right) \\ &\quad + \frac{2}{3} \left(\frac{1}{2} g_{\alpha\beta} + \frac{k_\alpha k_\beta}{m_f^2} \right) \left(\frac{1}{2} g_{\gamma\delta} + \frac{k_\gamma k_\delta}{m_f^2} \right). \end{aligned} \quad (82)$$

The ρ field also has a k -dependent term in the unitary gauge propagator [41],

$$iR_{\mu\nu}(k) = \frac{i}{k^2 - m_\rho^2 + im_\rho\Gamma_\rho} \left[-g_{\mu\nu} + \frac{k_\mu k_\nu}{m_\rho^2} \right], \quad (83)$$

but this term contributes to matrix elements only in the form $(m_a^2 - m_1^2)(m_b^2 - m_2^2)$ etc. and is thus zero for equal pion masses.

For t - and u -channel exchange of an α -meson ($\alpha = \sigma, \rho, f$) with momentum k by the pions, we implement monopole strong form factors [42]

$$h_\alpha(k) = \frac{m_\alpha^2 - m_\pi^2}{m_\alpha^2 - k^2}. \quad (84)$$

In Figure 4, we show the results of fitting this model to the elastic scattering data as before [22] but with the different propagator (82). Again, the fit is reasonably good, but the strong dependence on momentum-dependent terms in the f propagator shows up in the region above the f peak. Best-fit values for the free parameters now are: $m_\sigma = 475$ MeV, $m_\rho = 775$ MeV, $m_f = 1220$ MeV; $m_\sigma g_\sigma = 3.1$, $g_\rho = 6.15$, $m_f g_f = 8.85$. Throughout, we take $m_\pi = 140$ MeV.

For the current-based approximations of Section V, the above lagrangian is all we need; for the complete cross section of Section VI, it must be augmented by internal photon emission pieces. This can be achieved by minimal substitution, thereby guaranteeing gauge invariance (for a similar approach, see the ‘‘Quantum Hadrodynamics’’ lagrangians of Ref. [41]). To the hadronic lagrangian (80) we therefore add

$$\mathcal{L}_{\text{em}} = \mathcal{L}_{\pi\pi\gamma} + \mathcal{L}_{\rho\rho\gamma} + \mathcal{L}_{\pi\pi\sigma\gamma} + \mathcal{L}_{\pi\pi\rho\gamma} + \mathcal{L}_{\pi\pi f\gamma}. \quad (85)$$

Details regarding these pieces and corresponding vertex factors can be found in the Appendix.

The $\rho\rho\gamma$ interaction results in a modified strong form factor for t - or u -channel charged ρ exchange. If h_k and h_l are the usual form factors at the $\pi\pi\rho(k)$ and $\pi\pi\rho(l)$ vertices respectively, with $k = l + q$, electromagnetic gauge invariance requires that the form factor for the emission of a photon by the ρ be

$$H(k, l) = \frac{uh_l^2 - vh_k^2}{(u - v)h_k h_l}, \quad (86)$$

where $u = k^2 - m_\rho^2 + im_\rho\Gamma_\rho$ and $v = l^2 - m_\rho^2 + im_\rho\Gamma_\rho$ are the respective ρ propagators. For the monopole form (84) of h this becomes [42,43]

$$H(k, l) = 1 + \left(\frac{m_\rho^2 - k^2 - im_\rho\Gamma_\rho}{m_\rho^2 - l^2} \right) + \left(\frac{m_\rho^2 - l^2 - im_\rho\Gamma_\rho}{m_\rho^2 - k^2} \right). \quad (87)$$

Note that we do not include strict Vector Meson Dominance coupling of the photons to vector mesons. This is equivalent to the introduction of electromagnetic form factors. For the specific application we are considering, small M 's, those would be ≈ 1 . For previous OBE models, see e.g. Refs. [29,44] and references therein.

VIII. RESULTS AND CONCLUSIONS

To summarize: the differential cross section for dilepton production as a function of invariant mass, $d\sigma_{hh\ell^+\ell^-}/dM$, can be found in a number of approximations and an exact way (within the limitations of the hadronic reaction model). The approximations are: the Rückl approximation (70), two approximations, Eqs. (71) and (72), based on a more careful derivation by Lichard, using the real and virtual photon currents respectively, and an approximation integrating the current covariantly in 3-phase space, Eq. (77). The “exact” formula is given by Eq. (79).

Of these, the Rückl and Lichard cross sections can be found easily and quickly within 2-phase space. The 3-phase space current approximation is somewhat more difficult but still uses 2-phase space hadronic matrix elements. Implementing the exact formulation (79) involves much more effort: if there are N diagrams contributing to a given reaction, the sum in (79) contains $N(N+1)/2$ terms. Since an individual term T_{mn} in (78) is itself a Dirac sum, only partial factorization of the overall sum is possible. Further complications arise from the presence of imaginary pieces in the matrix elements.

To quantify the differences between the approximations and the exact formulation, we have studied all five distinct pion-pion reactions. Writing $(+-) \rightarrow (+-)$ as shorthand for the reaction $(\pi^+\pi^- \rightarrow \pi^+\pi^-\ell^+\ell^-)$ and so on, we have calculated within our OBE model cross sections for $(+-) \rightarrow (+-)$, $(++) \rightarrow (++)$, $(+-) \rightarrow (00)$, $(00) \rightarrow (+-)$ and $(+0) \rightarrow (+0)$. A total of 36 diagrams contribute at tree level to the first two reactions (24 for γ^* emitted by external pion lines, 12 by vertices and the exchange meson); the remaining reactions are made up of 16 diagrams each (8 external, 8 internal).

Numerical results were checked by performing the following consistency checks: setting $s_1 \rightarrow s$, $t_1 \rightarrow t$, $t_2 \rightarrow m_\pi^2$, $s_2 \rightarrow m_\pi^2$ and $M^2 \rightarrow 0$ in the *hadronic* part of the exact matrix elements (while keeping these variables where they enter the “current” part) and using only the external-emission diagrams reproduces exactly the results of the 3-phase space integrated current (77). Gauge invariance in the σ , ρ and f fields provided another sensitive test.

Figures 5–9 show the cross sections for these five reactions as a function of \sqrt{s} . In every case, the left and right panels show $d\sigma/dM$ for $M = 10$ MeV and 300 MeV respectively. Final-state symmetrization factors were included where appropriate. Initial-state symmetrization was also included for $(++) \rightarrow (++)$ and $(00) \rightarrow (+-)$ in order to facilitate use within a thermal pion gas environment. When the initial-state pions are considered distinguishable, these two cross sections should be multiplied by a factor 2 for these reactions.

Because they are identical in structure to their charge-conjugate versions, cross sections for the reactions $(+0) \rightarrow (+0)$ and $(++) \rightarrow (++)$ were doubled — this, too, should be corrected for when desired.

To prevent overcrowding, only the Rückl plus the virtual- γ^* current approximations (72) and (77) are shown, together with the exact calculations. All these were computed using the same OBE model and parameter values specified in Section VII above.

In the complicated structures and deviations in Figs. 5–9, the following points are of interest:

1. The ρ peak in the reaction $(+-) \rightarrow (+-)$ is overestimated by a factor 2.5 and 1.5 by the Rückl and Lichard approximations respectively for $M = 10$ MeV; for $M = 300$ MeV, the overestimation is much greater (Figure 5). Only the 3-space current approximation does an adequate job here. Similarly, the f peak of the exact result lies well below the corresponding approximations. Overestimation (1.7–5.0) of the ρ peak also occurs for approximations in $(+0) \rightarrow (+0)$.
2. In the reaction $(+0) \rightarrow (+0)$, the 3-space current approximation, on the other hand, lies well below the exact result (Figure 6).
3. Overestimation factors for $d\sigma/dM$ are of order 0.5–4 for the reactions $(00) \rightarrow (+-)$ and $(+-) \rightarrow (00)$, depending on approximation and cms energy. Here, too, the 3-space current approximation generally does better than the others but again tends to underestimate in some parts (Figs. 7, 8).
4. The largest discrepancy between approximations and the exact result occur for the reaction $(++) \rightarrow (++)$ (Figure 9): for the Rückl approximation, factors 3 (for 10 MeV) to 30 (for 300 MeV) arise, while the Lichard approximation yields corresponding overestimation factors of 1.9 and 14–20. Since, however, this reaction contributes only little when contributions from all reactions are added up, this effect is not of much interest in a heavy-ion context.
5. There is generally not much difference between using the real-photon (not shown) or virtual-photon currents in the Lichard approximations; this is in agreement with the conclusions of Ref. [27]. For $M = 300$ MeV, some differences can be discerned, but both deviate in general more from the exact result than from each other.

Figures 10 and 11 show the dilepton production rates per unit spacetime summed over all seven reactions, calculated using the Boltzmann formula (37), for temperatures $T = 100$ and 200 MeV respectively. These temperatures probably lie below and above an expected transition to a new quark-gluon phase and so represent extrema in their behavior. Corresponding ratios of approximation over exact rates are shown in Figures 12 and 13. The Rückl approximation is the worst, as expected; overestimation is in the range 2–4 for $T = 100$ MeV, and 2–8 for $T = 200$ MeV. The Lichard approximations overestimate by factors 1.4–4, depending on temperature and s . Here, the *real- γ* 3-phase space current, the lower of the two dotted lines, does surprisingly well, deviating from the exact result by less than 20% throughout. Comparing this fact, however, with the substantial deviations shown in the s -differential cross sections of Figs. 5–9, one must conclude that much of the “agreement” seen on the

level of rates is due to averaging over differences seen in the s -dependent cross sections and that such “agreement” therefore does not validate the approximations.

We also note the fact that none of the approximations approaches the exact result for small values of M : even for the smallest value shown ($M = 10$ MeV), the discrepancy is still above 40% for the Lichard approximations and larger than a factor 2 for the Rückl approximation.

Figure 14 shows the fractional contributions to the total $T = 200$ MeV rate for the Rückl, virtual- γ current Lichard, and exact cross sections. As discussed, the $(++) \rightarrow (++)$ contribution virtually falls away in the exact calculation; by contrast the reaction $(+0) \rightarrow (+0)$ plus charge conjugate becomes more important, in second place behind the dominant reaction $(+-) \rightarrow (+-)$.

Finally, we ask where the discrepancies between approximations and exact cross section originate: is this due to the inclusion of diagrams with photon emission from vertices and propagators? A partial answer is provided by Figure 15, where the cross sections for reactions $(++) \rightarrow (++)$ and $(+-) \rightarrow (00)$ are plotted. The upper lines correspond, as before, to the Rückl and two Lichard approximations, while the solid line again represents the exact result. The lowest dash-dotted line, on the other hand, represents the exact result but excluding all internal diagrams and their cross terms with external ones. The difference between this lower line and the exact result (solid line) therefore represents the contribution of the internal diagrams; while the difference between the lower dash-dotted line and the upper lines (approximations) represents the change in cross section due to inclusion/exclusion of q in the *external*-emission diagrams.

We see that the contribution of internal emission is not all that large, albeit nonnegligible. By far the most important effect on $d\sigma/dM$ is the inclusion of the full dependence of \mathcal{M} on the photon momentum q . In fact, the effect is so large that for the reaction $(++) \rightarrow (++)$ the cross section would become negative⁴ if internal diagrams were not included! In other words, among the list of approximations listed in Section II B, approximation (B) is the most far-reaching.

The importance of including q fully in the matrix element can be understood qualitatively: as illustrated in Figs. 5–9 for one reaction, the elastic pion-pion cross sections vary considerably within the region of interest. Adding or subtracting a sizeable amount of energy-momentum in the form of q therefore naturally leads to a substantial change in cross section also. This change is, however, neglected in all the approximations listed⁵. We believe that this (unavoidable) neglect is at the heart of the considerable differences between approximations and exact result seen in Figs. 5–9.

In summary, the various approximations for bremsstrahlung from pion-pion collisions

⁴ Since this curve does not represent a gauge-invariant calculation, this negative cross section is of no physical consequence. In fact, it illustrates once again the necessity of including internal diagrams to make the cross section positive again.

⁵ This also explains why the overestimation is so large for the reaction $(++) \rightarrow (++)$: there are no resonances in the cross section which could provide some amount of cancellation by pion-pion reactions being “shifted into” and “shifted out of” a resonance peak.

cannot in general be believed beyond at best a factor 2 or more, depending on invariant mass and temperature.

We have shown in Sections III B and VI how 3-phase space can be fully taken into account. The most important effect, it turns out, is not the inclusion of photon emission from vertices or propagators but the strong dependence of the cross section on the inclusion of the photon momentum q into the *hadronic* collision part.

Since this calculation neglected baryonic degrees of freedom and resonances, and because of the technical difficulties of a further integration over spacetime, our results are not applied directly to experimental data; this is a matter for the future. All we can say at this stage is that it is likely that the approximations overestimate the dilepton yield throughout the mass region of interest, and that the degree of overestimation rises both with increasing invariant mass M and temperature T . Since the bremsstrahlung channel competes with various Dalitz decays, and since various experiments take much care in applying cuts to eliminate Dalitz pairs as far as possible [12] a quantitative estimate would necessarily have to take such experimental cuts into account also.

In addition, attention should be paid to the issue of the Landau-Pomeranchuk effect, which is expected to suppress dilepton bremsstrahlung rates [24,25,28]. Our results, taken in conjunction with these calculations, therefore appear to indicate even larger suppression of bremsstrahlung dileptons than had been thought previously.

ACKNOWLEDGMENTS

We thank P. Lichard for enlightening discussions and his careful derivation of dilepton formulas. Thanks to A. Drees, J. Zhang, J. C. Pan, P. Lipa and B. Buschbeck for useful discussions. This work was supported in part by the Natural Sciences and Engineering Research Council of Canada, by the Québec FCAR fund, by a NATO Collaborative Research Grant, by the National Science Foundation under grant number 94-03666 and by the Austrian Fonds zur Förderung der wissenschaftlichen Forschung (FWF).

APPENDIX: FULL OBE LAGRANGIAN

Besides the hadronic interaction lagrangian (80) with its vertex factors

$$\begin{aligned}
\Gamma_{\pi\pi\sigma} &= \begin{cases} 2ig_\sigma p \cdot p' & \text{for } \pi^\pm(p) \rightarrow \pi^\pm(p') \sigma \\ ig_\sigma p \cdot p' & \text{for } \pi^0(p) \rightarrow \pi^0(p') \sigma \end{cases} \\
\Gamma_{\pi\pi\rho} &= \begin{cases} \mp ig_\rho (p + p')^\mu & \text{for } \pi^\pm(p) \rightarrow \pi^\pm(p') \rho_0^\mu \\ \pm ig_\rho (p + p')^\mu & \text{for } \pi^\pm(p) \rightarrow \pi^0(p') \rho_\pm^\mu \\ \pm ig_\rho (p + p')^\mu & \text{for } \pi^0(p) \rightarrow \pi^\pm(p') \rho_\mp^\mu \end{cases} \\
\Gamma_{\pi\pi f} &= \begin{cases} ig_f (p^\alpha p'^\beta + p^\beta p'^\alpha) & \text{for } \pi^\pm(p) \rightarrow \pi^\pm(p') f^{\alpha\beta} \\ ig_f p^\alpha p'^\beta & \text{for } \pi^0(p) \rightarrow \pi^0(p') f^{\alpha\beta} \end{cases}
\end{aligned} \tag{A1}$$

we need the electromagnetic interaction lagrangian linear in A_μ ,

$$\mathcal{L}_{\text{em}} = \mathcal{L}_{\pi\pi\gamma} + \mathcal{L}_{\rho\rho\gamma} + \mathcal{L}_{\pi\pi\sigma\gamma} + \mathcal{L}_{\pi\pi\rho\gamma} + \mathcal{L}_{\pi\pi f\gamma}. \tag{A2}$$

With the pion current

$$j_\pi^\mu \equiv i(\pi^- \partial^\mu \pi^+ - \pi^+ \partial^\mu \pi^-), \quad (\text{A3})$$

the $\boldsymbol{\rho}$ field tensor,

$$\mathbf{B}^{\mu\nu} \equiv \partial^\mu \boldsymbol{\rho}^\nu - \partial^\nu \boldsymbol{\rho}^\mu - g_\rho \boldsymbol{\rho}^\mu \times \boldsymbol{\rho}^\nu, \quad (\text{A4})$$

and $F_{\mu\nu} \equiv \partial_\mu A_\nu - \partial_\nu A_\mu$ the usual electromagnetic tensor, the individual contributions are

$$\mathcal{L}_{\pi\pi\gamma} = -eA_\mu j_\pi^\mu, \quad (\text{A5})$$

$$\mathcal{L}_{\rho\rho\gamma} = eA_\mu [\boldsymbol{\rho}_\nu \times \mathbf{B}^{\mu\nu}]_3 + \frac{1}{2} e F_{\mu\nu} [\boldsymbol{\rho}^\mu \times \boldsymbol{\rho}^\nu]_3 \quad (\text{A6})$$

$$= ieA_\mu [\rho_{-\nu} (\partial^\mu \rho_+^\nu - \partial^\nu \rho_+^\mu) - \rho_{+\nu} (\partial^\mu \rho_-^\nu - \partial^\nu \rho_-^\mu)] + ie \partial_\mu A_\nu [\rho_-^\mu \rho_+^\nu - \rho_-^\nu \rho_+^\mu],$$

$$\mathcal{L}_{\pi\pi\sigma\gamma} = -2eg_\sigma A_\mu j_\pi^\mu, \quad (\text{A7})$$

$$\mathcal{L}_{\pi\rho\pi\gamma} = -eg_\rho A_\mu [\boldsymbol{\pi} \times (\boldsymbol{\pi} \times \boldsymbol{\rho}^\mu)]_3 \quad (\text{A8})$$

$$= eg_\rho A_\mu [2\pi^+ \pi^- \rho_0^\mu - \pi^- \pi^0 \rho_+^\mu - \pi^+ \pi^0 \rho_-^\mu],$$

$$\mathcal{L}_{\pi\pi f\gamma} = -eg_f f_{\mu\nu} [A^\mu j_\pi^\nu + A^\nu j_\pi^\mu]. \quad (\text{A9})$$

The corresponding vertex factors are

$$\begin{aligned} \Gamma_{\pi\pi\gamma} &= \mp ie(p+p')^\mu && \text{for } \pi^\pm(p) \rightarrow \pi^\pm(p') A^\mu \\ \Gamma_{\rho\rho\gamma} &= \pm ie [g^{\alpha\beta}(p+p')^\mu - g^{\alpha\mu} p'^\beta - g^{\beta\mu} p^\alpha] && \text{for } \rho_\pm^\alpha(p) \rightarrow \rho_\pm^\beta(p') A^\mu(q) \\ \Gamma_{\pi\pi\sigma\gamma} &= \pm 2ieg_\sigma(p+p')^\mu && \text{for } \pi^\pm(p) \rightarrow \pi^\pm(p') \sigma A^\mu \\ \Gamma_{\pi\rho\pi\gamma} &= \begin{cases} -2ieg_\rho g^{\mu\nu} & \text{for } \pi^\pm(p) \rightarrow \pi^\pm(p') \rho_0^\nu A^\mu \\ +ieg_\rho g^{\mu\nu} & \text{for } \pi^\pm(p) \rightarrow \pi^0(p') \rho_\pm^\nu A^\mu \\ +ieg_\rho g^{\mu\nu} & \text{for } \pi^0(p) \rho_\pm^\nu \rightarrow \pi^\pm(p') A^\mu \end{cases} && (\text{A10}) \\ \Gamma_{\pi\pi f\gamma} &= \pm ieg_f [g^{\alpha\mu}(p+p')^\beta + g^{\beta\mu}(p+p')^\alpha] && \text{for } \pi^\pm(p) \rightarrow \pi^\pm(p') f^{\alpha\beta} A^\mu. \end{aligned}$$

REFERENCES

- [1] E.L. Feinberg, Nuov. Cim. **34A**, 39 (1976).
- [2] E.V. Shuryak, Phys. Lett. **78B**, 150 (1978).
- [3] K. Kajantie, J. Kapusta, L. McLerran and A. Mekjian, Phys. Rev. **D34**, 2746 (1986).
- [4] Proceedings of the 11th International Conference on Ultrarelativistic Nucleus-Nucleus Collisions, Monterey, CA, Jan. 9-13, 1995, Nucl. Phys. **A590**, 1c (1995).
- [5] M.R. Adams et al., Phys. Rev. **D27**, 1977 (1983).
- [6] D. Blockus et al., Nucl. Phys. **B201**, 205 (1982).
- [7] S. Mikamo et al., Phys. Lett. **106B**, 428 (1981).
- [8] G. Roche, Talk presented at the NATO Advanced Study Institute, Bodrum/Turkey, September 1993, and references therein; in: Proceedings of the NATO ASI on Hot and Dense Nuclear Matter, edited by W. Greiner, H. Stöcker and A. Gallmann, NATO ASI Series B335.
- [9] HELIOS-3 Collaboration, T. Åkesson et al., Z. Phys. **C68**, 47 (1995).
- [10] NA45/CERES Collaboration, G. Agakichiev et al., Phys. Rev. Lett. **75**, 1272 (1995).
- [11] NA38 Collaboration, C. Lourenco et al., in Ref. [4].
- [12] I. Tserruya; preprint CERN-PPE/95-52, in Ref. [4].
- [13] R. Vogt, B.V. Jacak, P.L. McGaughey and P.V. Ruuskanen, Phys. Rev. **D49**, 3345 (1994).
- [14] C. Gale and P. Lichard, Phys. Rev. **D49**, 3338 (1994).
- [15] P. Lichard, Phys. Rev. **D49**, 5812 (1994).
- [16] See, for example, C. Y. Wong, *Introduction to high-energy heavy-ion collisions*, World Scientific, Singapore (1994).
- [17] C. Gale and J.I. Kapusta, Phys. Rev. **D35**, 2107 (1987).
- [18] J. Cleymans, K. Redlich and H. Satz, Z. Phys. **C52**, 517 (1991).
- [19] M. Schäfer, T. Biró, W. Cassing and U. Mosel, Phys. Lett. **221B**, 1 (1994).
- [20] Gy. Wolf, et al., Nucl. Phys. **A517**, 615 (1990).
- [21] K. Haglin, C. Gale and V. Emel'yanov, Phys. Rev. **D46**, 4082 (1992).
- [22] K. Haglin, C. Gale and V. Emel'yanov, Phys. Rev. **D47**, 973 (1993).
- [23] P. Koch, Z. Phys. **C57**, 283 (1993).
- [24] J. Cleymans, V.V. Goloviznin and K. Redlich, Phys. Rev. **D47**, 173 (1993).
- [25] J. Cleymans, V.V. Goloviznin and K. Redlich, Phys. Rev. **D47**, 989 (1993).
- [26] P. Lichard, Phys. Rev. **D51**, 6017 (1995).
- [27] J. Zhang, R. Tabti, C. Gale and K. Haglin, preprint MCGILL/94-56; R. Tabti, MSc thesis, McGill University 1995 (unpublished).
- [28] J. Knoll and D.N. Voskresenskii, Phys. Lett. **351B**, 43 (1995).
- [29] K. Haglin, Ann. Phys. (NY) **212**, 84 (1991).
- [30] J.D. Bjorken and S. Drell, *Relativistic Quantum Mechanics*, McGraw-Hill, New York (1964).
- [31] F. Low, Phys. Rev. **110**, 974 (1958).
- [32] R. Rückl, Phys. Lett. **64B**, 39 (1976).
- [33] J. Alam, D.K. Srivastava, B. Sinha, and D.N. Basu, Phys. Rev. **D48**, 1117 (1993).
- [34] N.S. Craigie and H.N. Thompson, Nucl. Phys. **B141**, 121 (1978).
- [35] E. Byckling and K. Kajantie, *Particle Kinematics*, (Wiley, London, 1973).
- [36] C. Gale and J.I. Kapusta, Phys. Rev. **C40**, 2398 (1989).

- [37] S.D. Protopopescu et al., Phys. Rev. **D7**, 1279 (1973).
- [38] V. Srinivasan et al., Phys. Rev. **D12**, 681 (1976).
- [39] H. van Dam and M. Veltman, Nucl. Phys. **B22**, 397 (1970).
- [40] M.J.G. Veltman, in: *Les Houches, Session XXVIII — Méthodes en théorie des champs*, edited by R. Balian and J. Zinn-Justin, North Holland (1976), pp. 267–327.
- [41] B.D. Serot and J.D. Walecka, *The relativistic nuclear many-body problem*, Advances in Nuclear Physics, Vol. 16, edited by J. W. Negele and E. Vogt, Plenum, New York (1986); B.D. Serot and J.D. Walecka, Rep. Prog. Phys. **55**, 1855 (1992).
- [42] D.O. Riska, Prog. Part. Nucl. Phys. **11**, 199 (1984).
- [43] I.S. Towner, Phys. Rep. **155**, 264 (1987).
- [44] M. Schäfer, H.C. Dönges, A. Engel and U. Mosel, Nucl. Phys. **A575**, 429 (1994).

List of Figures

Figure 1: Breakdown of the soft photon approximation: the SPA is valid only when q_0 is much smaller than the two solid lines shown. The region between the dashed lines is the domain of integration for q_0 when calculating cross sections as a function of dilepton invariant mass.

Figure 2: One of the four contributing diagrams following from SPA factorization of the matrix element into leptonic tensor $L_{\mu\nu}$, photon emission current J^μ , and elastic hadronic matrix element \mathcal{M}_h .

Figure 3: Relativistic invariants for three-particle final state phase space.

Figure 4: OBE model fitted to the elastic $\pi^+\pi^- \rightarrow \pi^+\pi^-$ cross section. Parameter values determined from this fit are used for all reactions throughout this paper.

Figure 5: Cross section for the reaction $\pi^+\pi^- \rightarrow \pi^+\pi^-e^+e^-$ as a function of \sqrt{s} for fixed dielectron invariant masses $M = 10$ and 300 MeV. Solid line: exact OBE calculation Eq. (79). Dash-dotted line: Rückl approximation (70) — this is the commonly-used version of the SPA. Other approximations are: Dashed line: angular-averaged virtual γ current (72). Dotted line: 3-phase space current (77).

Figure 6: Same as Figure 5, for the reactions $\pi^+\pi^0 \rightarrow \pi^+\pi^0e^+e^-$ plus $\pi^-\pi^0 \rightarrow \pi^-\pi^0e^+e^-$

Figure 7: Same as Figure 5, for the reaction $\pi^+\pi^- \rightarrow \pi^0\pi^0e^+e^-$, including final-state symmetry factor. Note the different scales on the y -axes.

Figure 8: Same as Figure 5, for the reaction $\pi^0\pi^0 \rightarrow \pi^+\pi^-e^+e^-$. An initial-phase space factor of $1/2$ is included.

Figure 9: Same as Figure 5, for the reactions $\pi^+\pi^+ \rightarrow \pi^+\pi^+e^+e^-$ plus $\pi^-\pi^- \rightarrow \pi^-\pi^-e^+e^-$. Initial- times final-state symmetry factors $(1/2)^2$ are included.

Figure 10: Total bremsstrahlung yield of e^+e^- for all seven pion-pion reactions, for a Boltzmann gas with temperature $T = 100$ MeV. Solid line: exact OBE calculation, Dash-dotted line: Rückl approximation, Dashed line: angular-averaged virtual- γ^* current, Dotted line: 3-phase space current, virtual- γ^* current (upper) real- γ current (lower).

Figure 11: Same as Figure 10, for temperature $T = 200$ MeV.

Figure 12: Ratios of SPA approximation calculations divided by exact OBE rate for $T = 100$ MeV. Dash-dotted line: Rückl/exact, Dashed line: (angular-averaged virtual γ current)/exact. Upper dotted line: (3-phase space virtual γ current)/exact. Lower dotted line: (3-phase space real γ current)/exact.

Figure 13: Same as Figure 12, for $T = 200$ MeV,

Figure 14: Fractional contribution to the total dielectron rate at $T = 200$ MeV as a function of dilepton invariant mass M for (a) the Rückl, (b) virtual-photon Lichard approximations and (c) the exact calculation. Solid line (upper): $(+-) \rightarrow (+-)$, Dashed line: $(+0) \rightarrow (+0)$ plus c.c., Solid line (lower): $(00) \rightarrow (+-)$, Dash-dotted line: $(+-) \rightarrow (00)$, Dotted line: $(++) \rightarrow (++)$ plus c.c.

Figure 15: Contribution of external-emission vs. external-plus-internal diagrams for the reactions $(+-) \rightarrow (00)$ (left) and $(++) \rightarrow (++)$ (right), both for $M = 300$ MeV. Lines are as in Figs. 7 and 9. The new dash-dotted line below the (solid line) exact calculation represents contributions arising solely from emission of γ^* by an external pion line, but taking q into account in \mathcal{M} , in contrast to the approximations (upper lines) which neglected q .

Figure 1

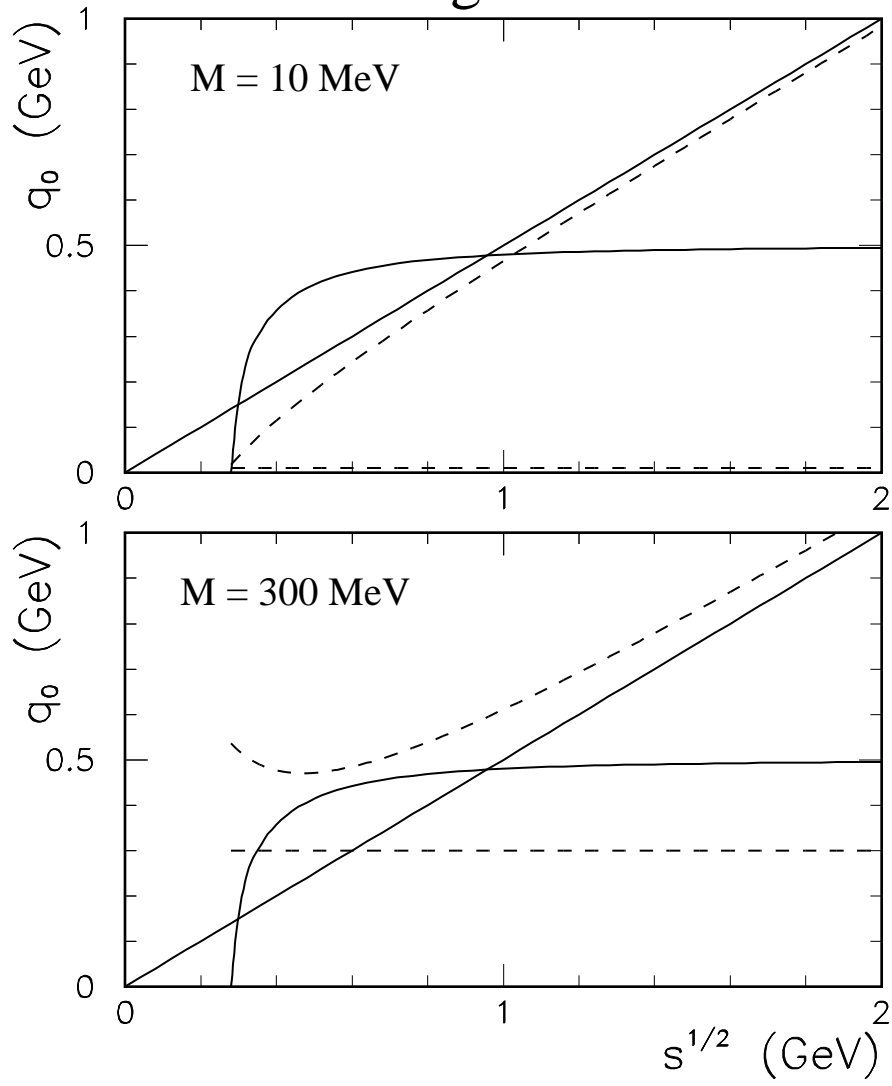


Figure 2

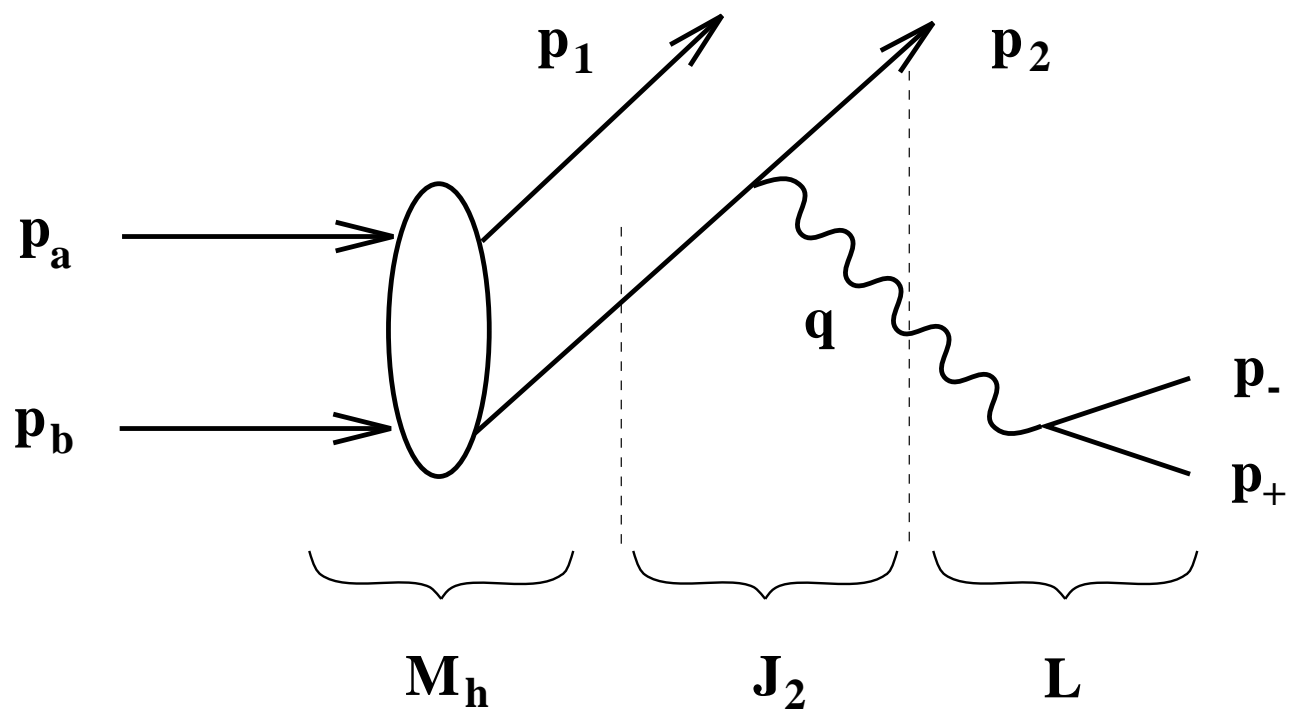
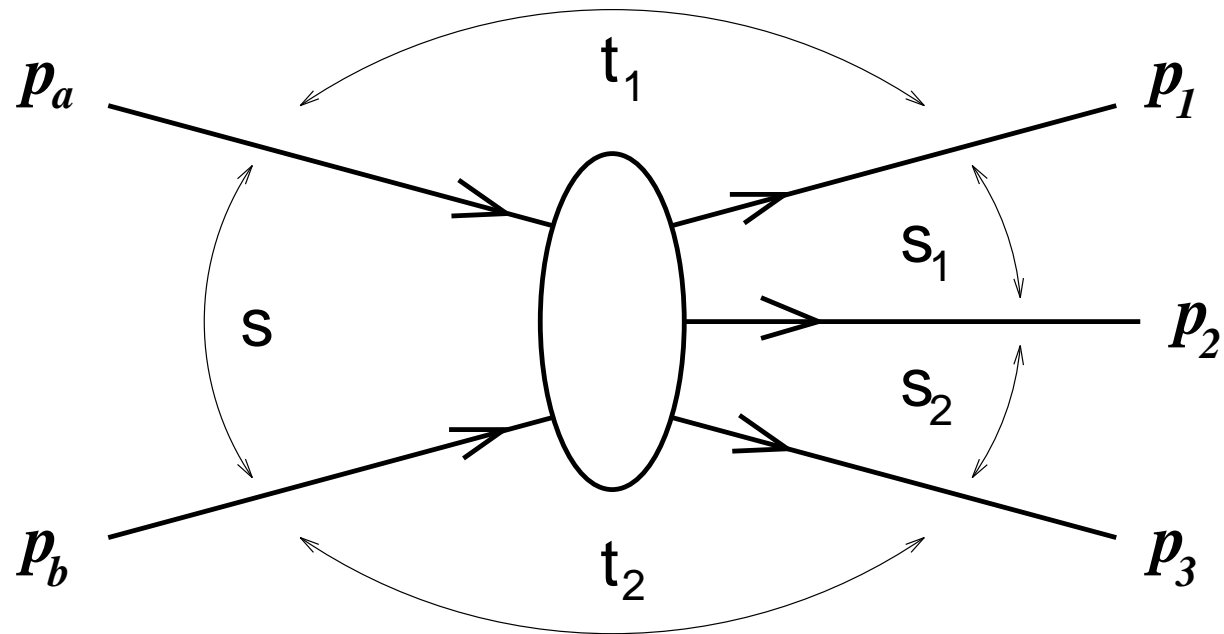


Figure 3



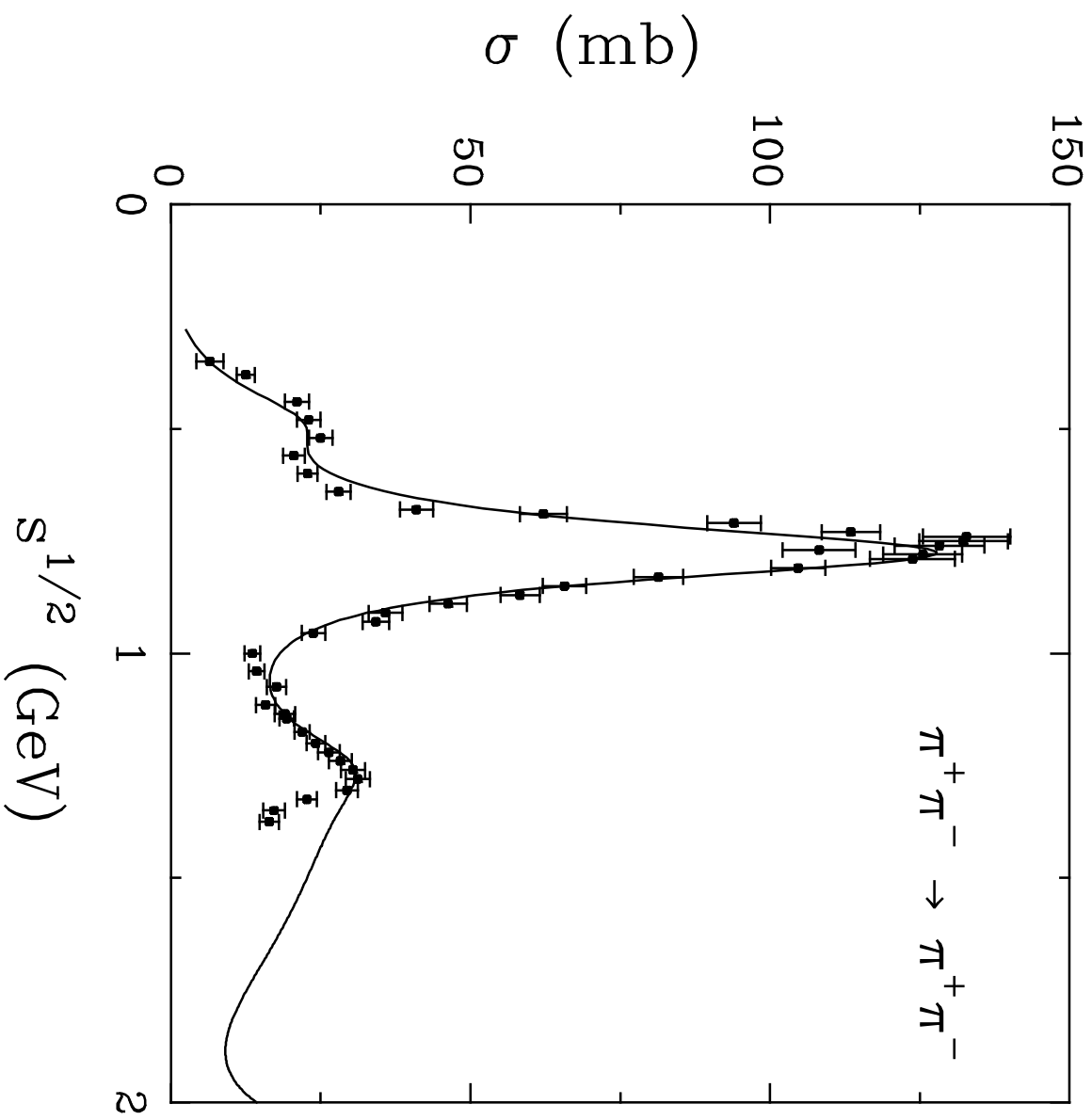


Figure 5

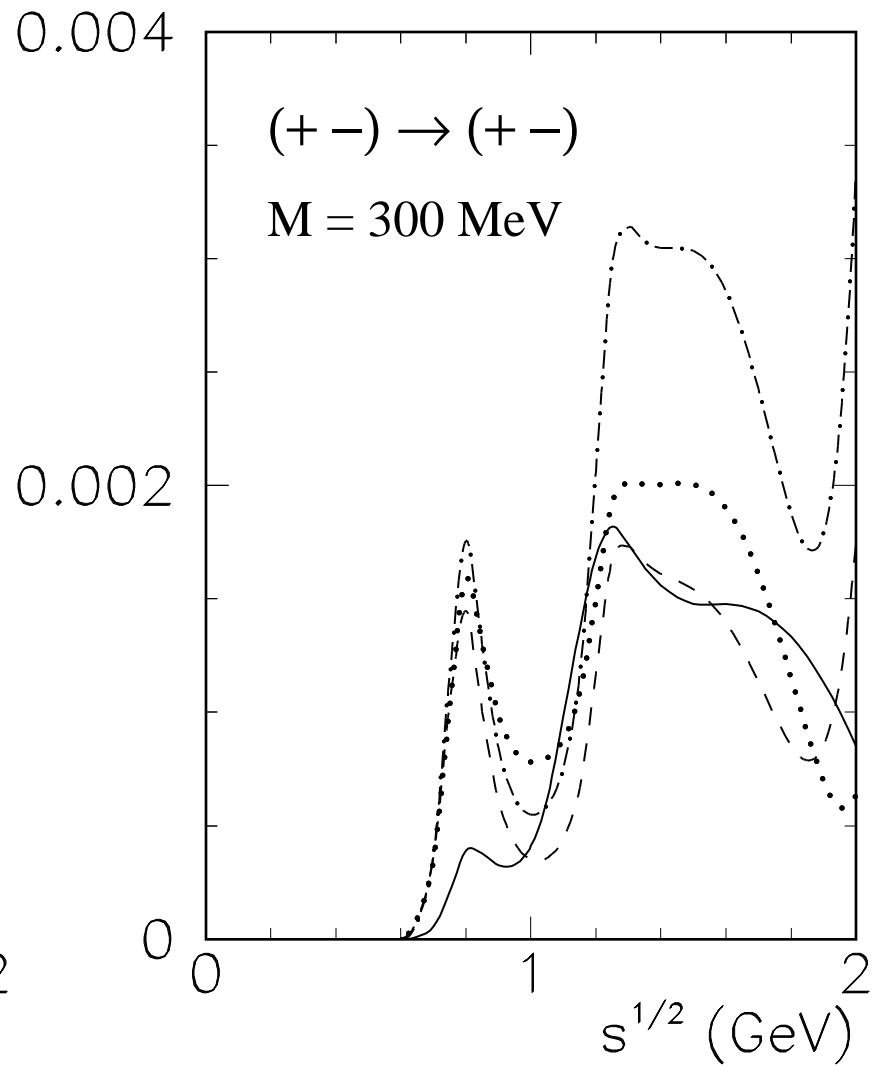
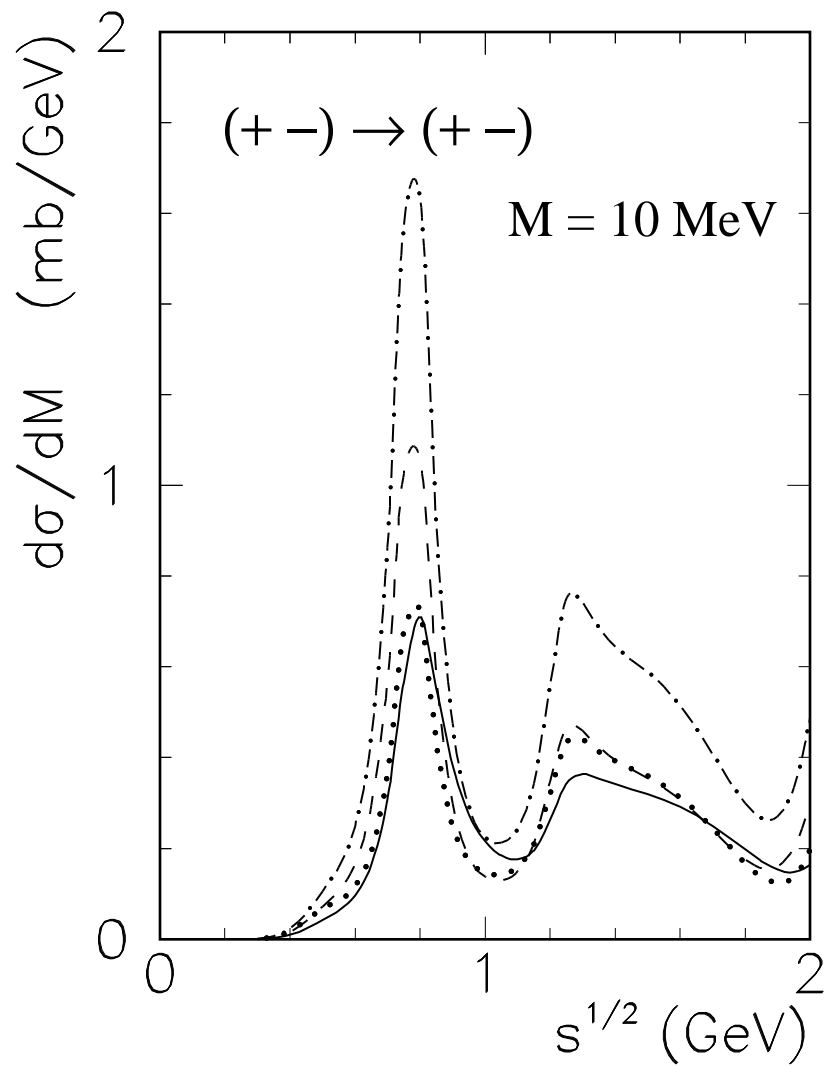


Figure 6

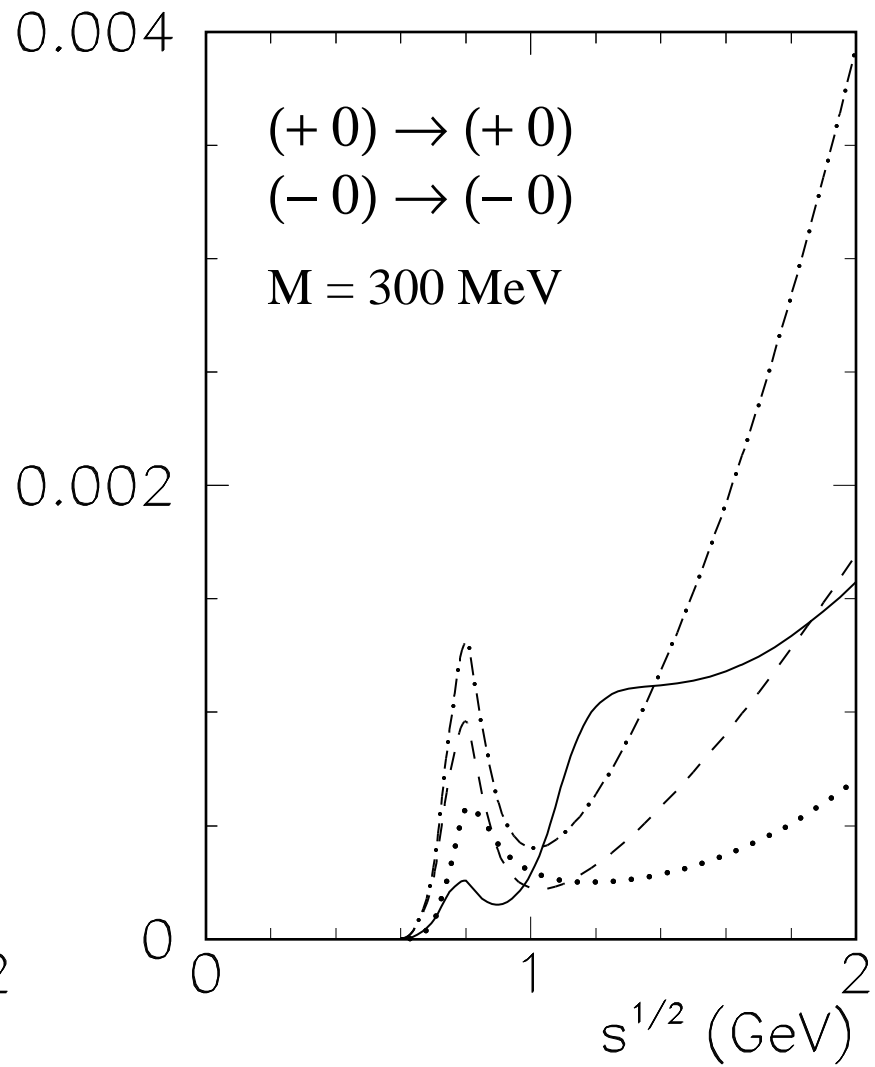
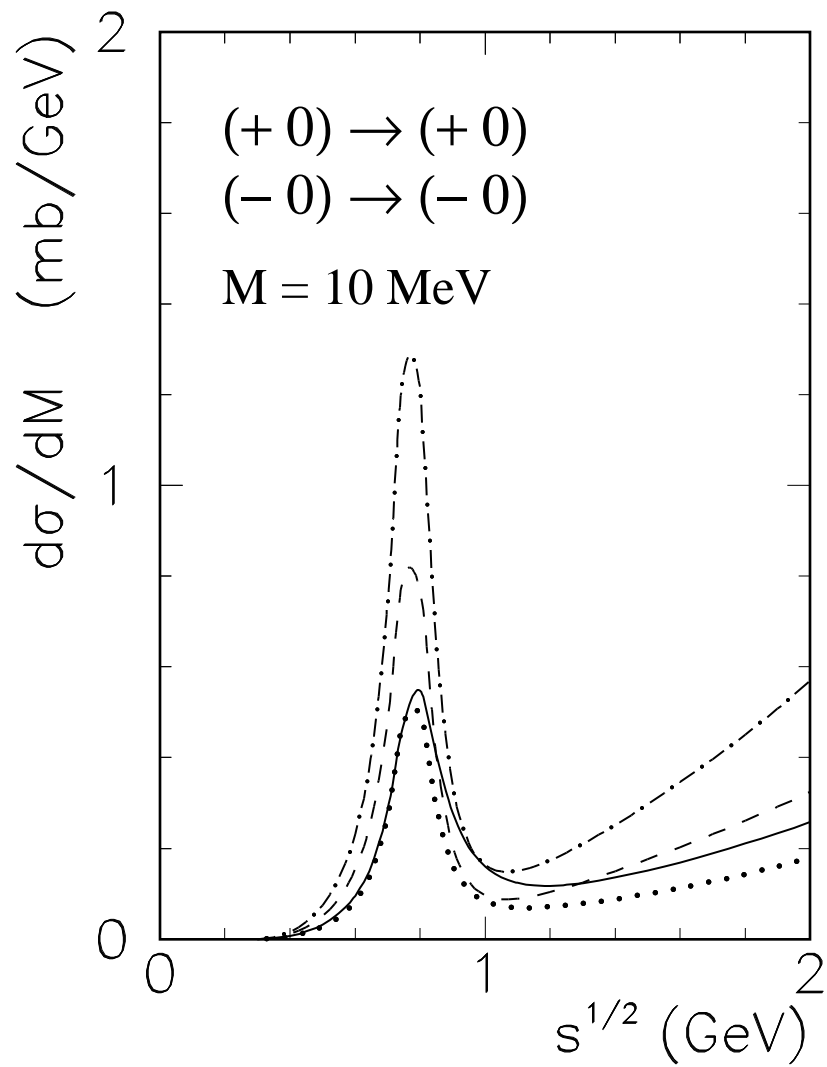


Figure 7

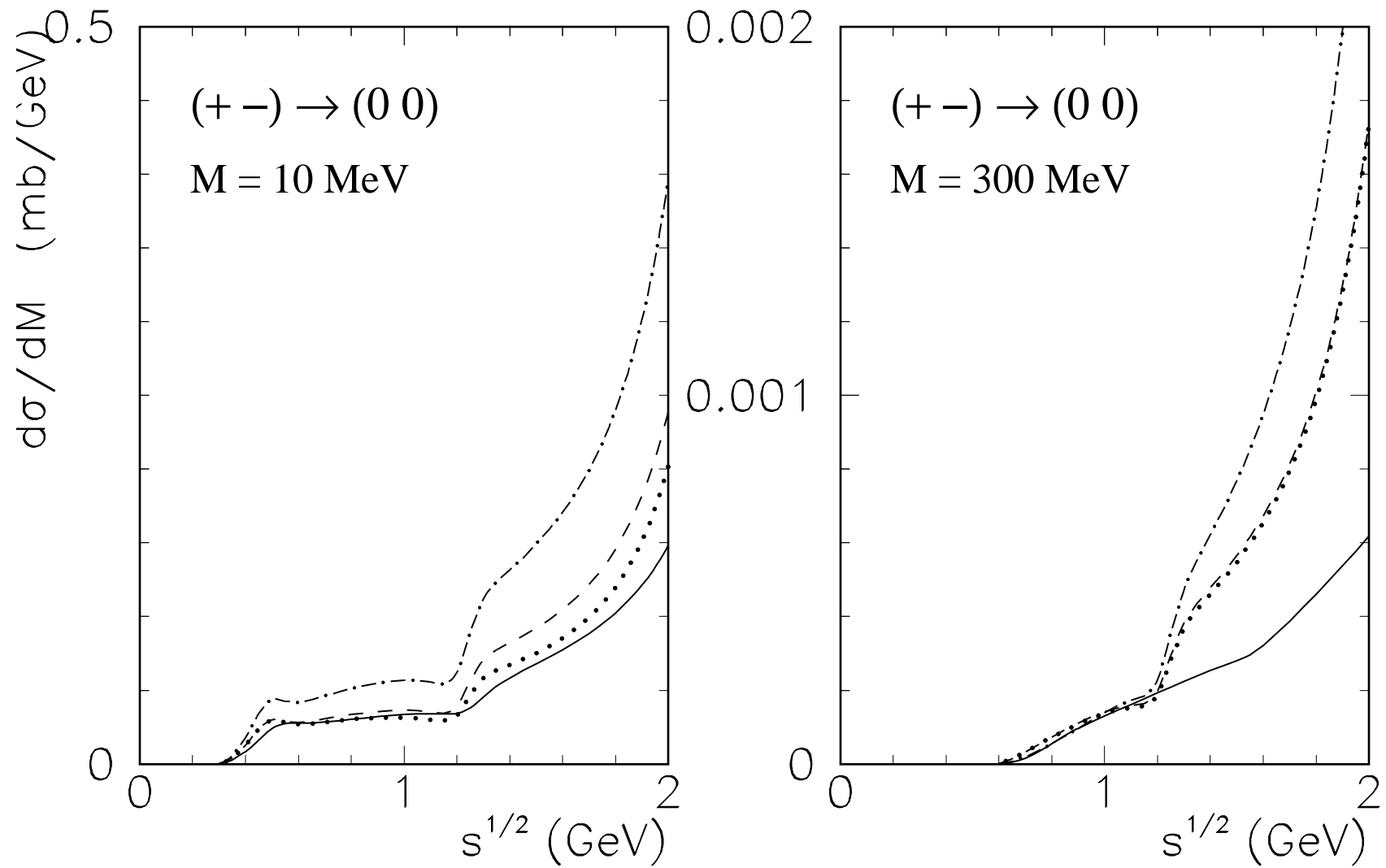


Figure 8

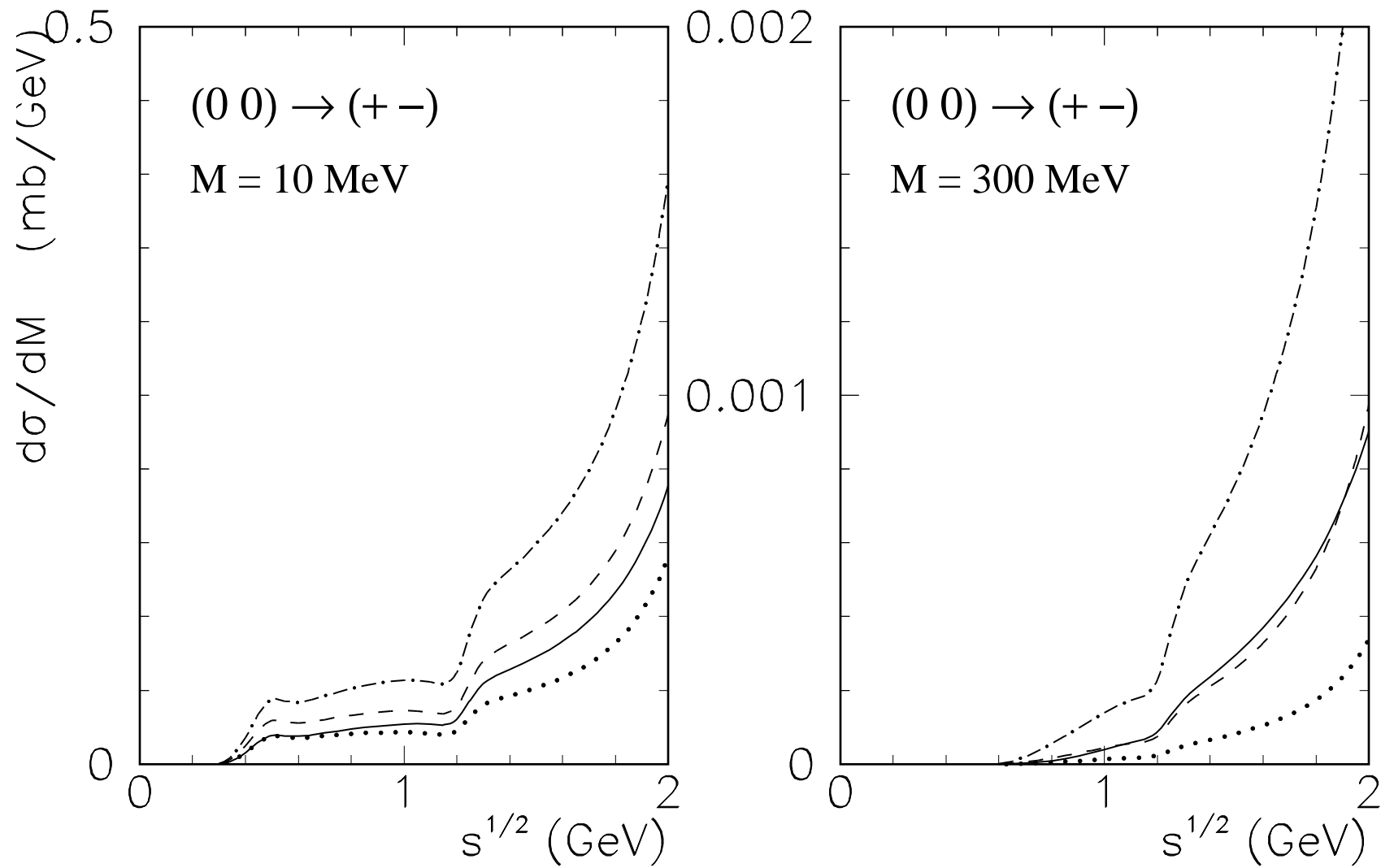


Figure 9

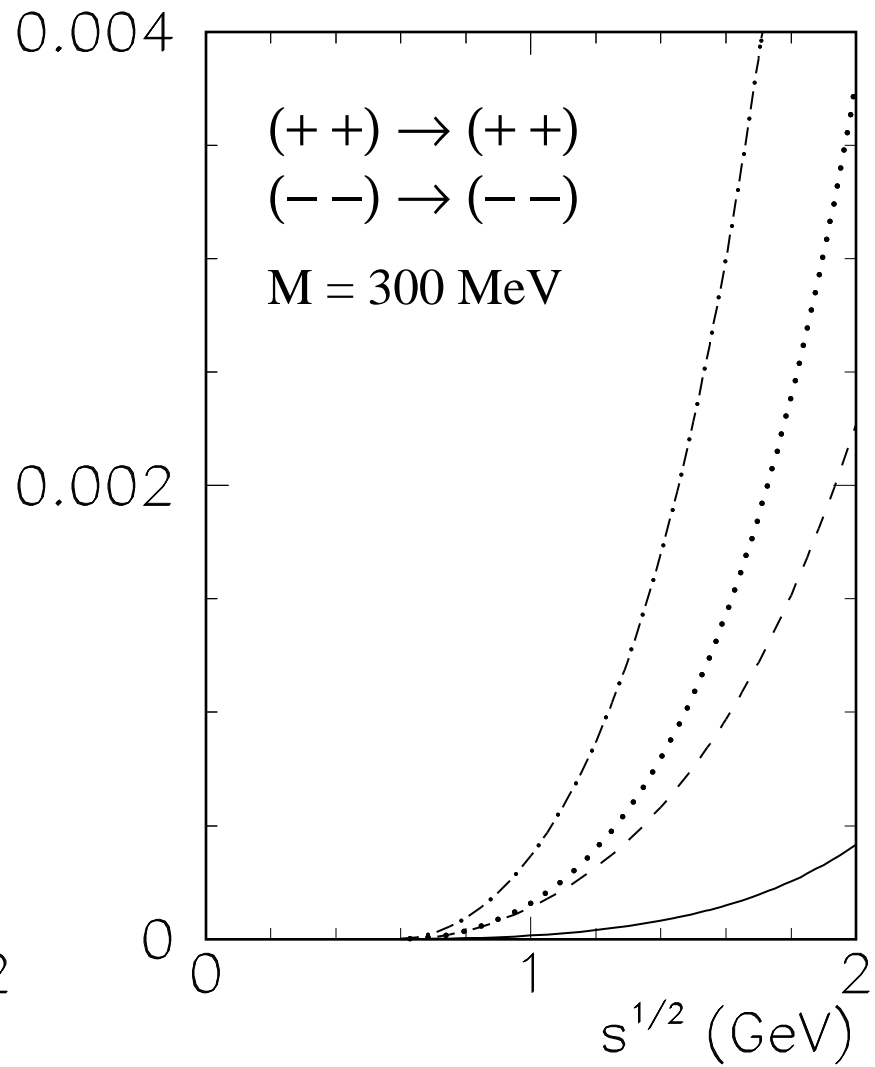
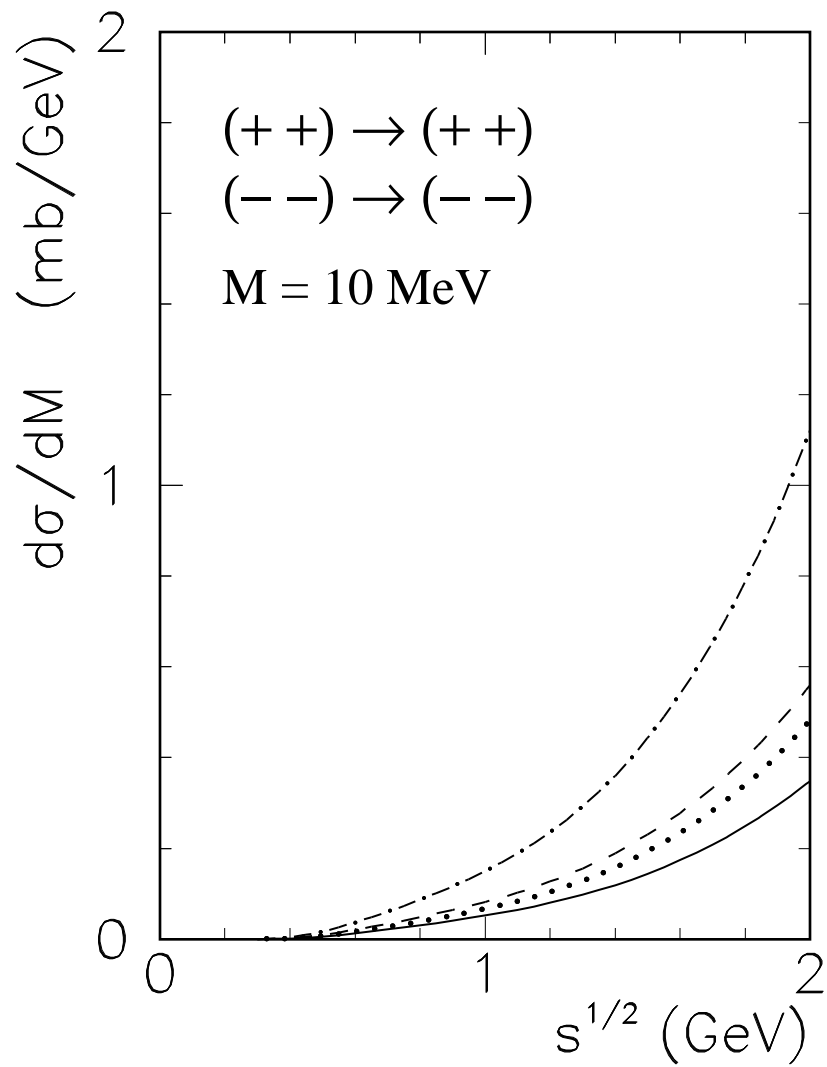


Figure 10

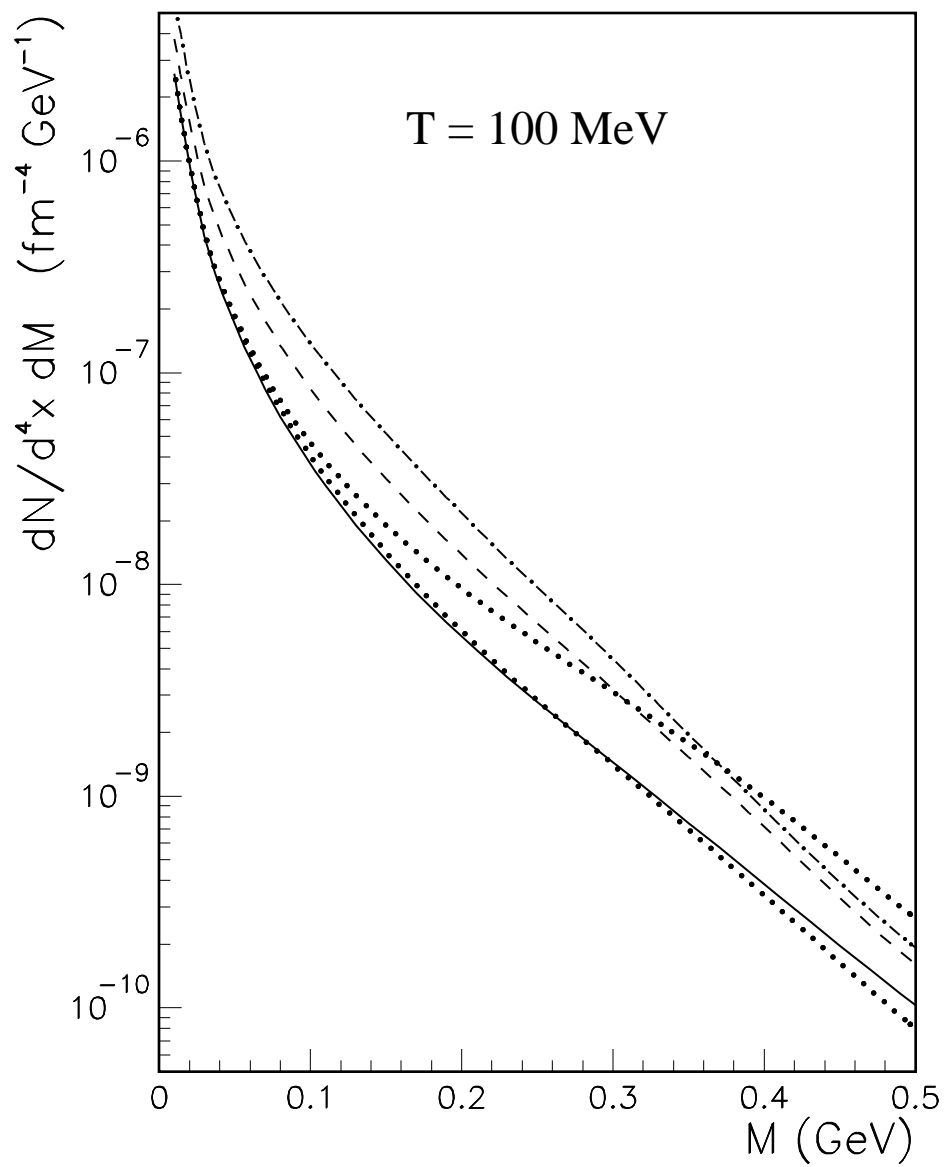


Figure 11

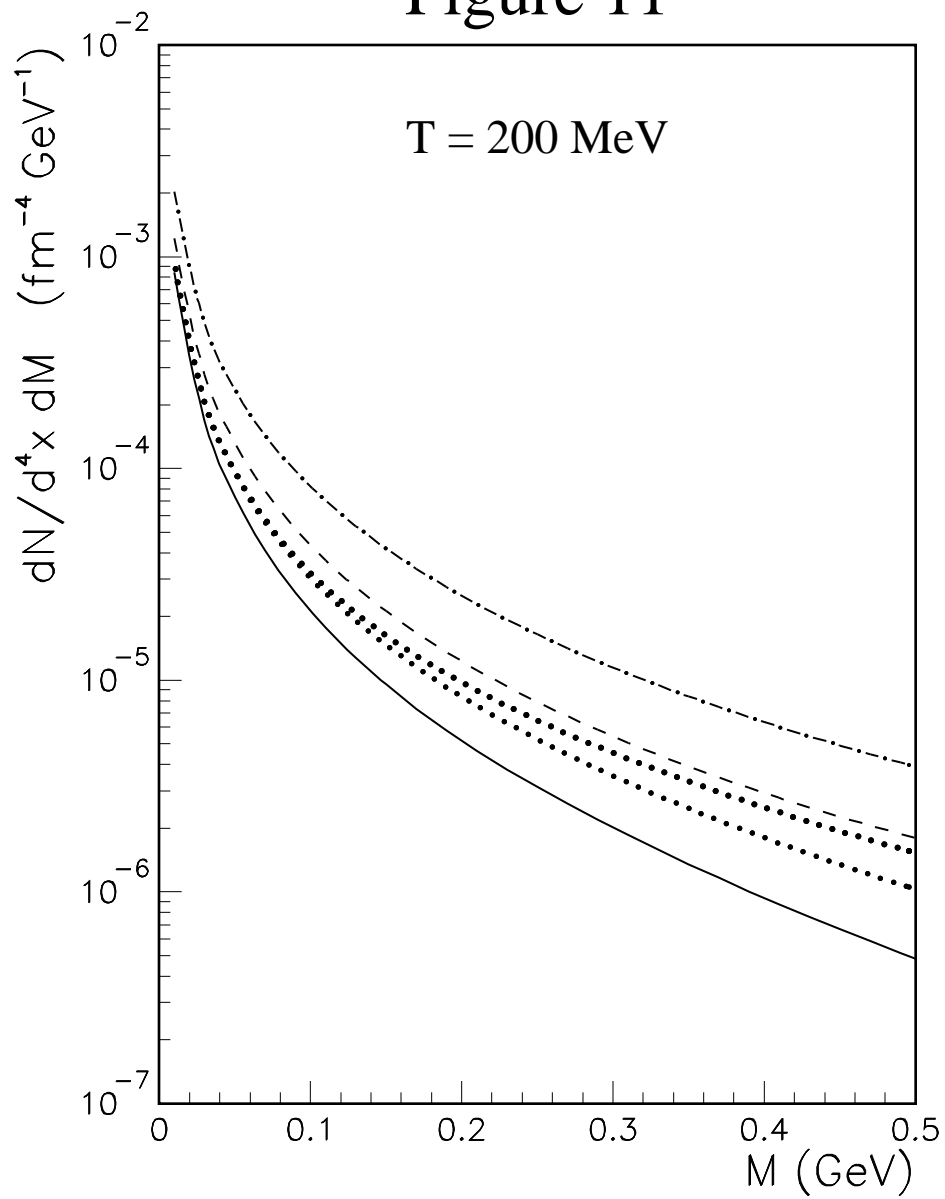


Figure 12

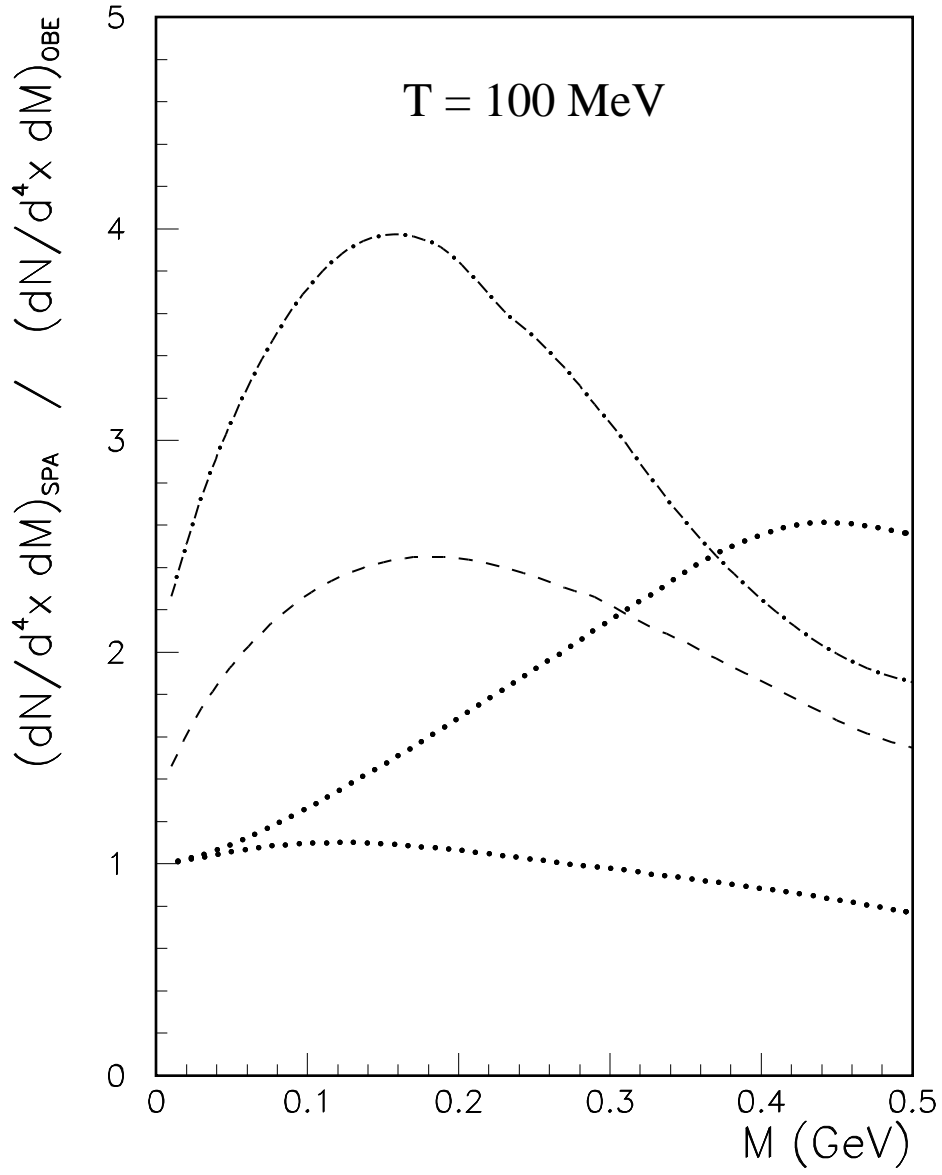


Figure 13

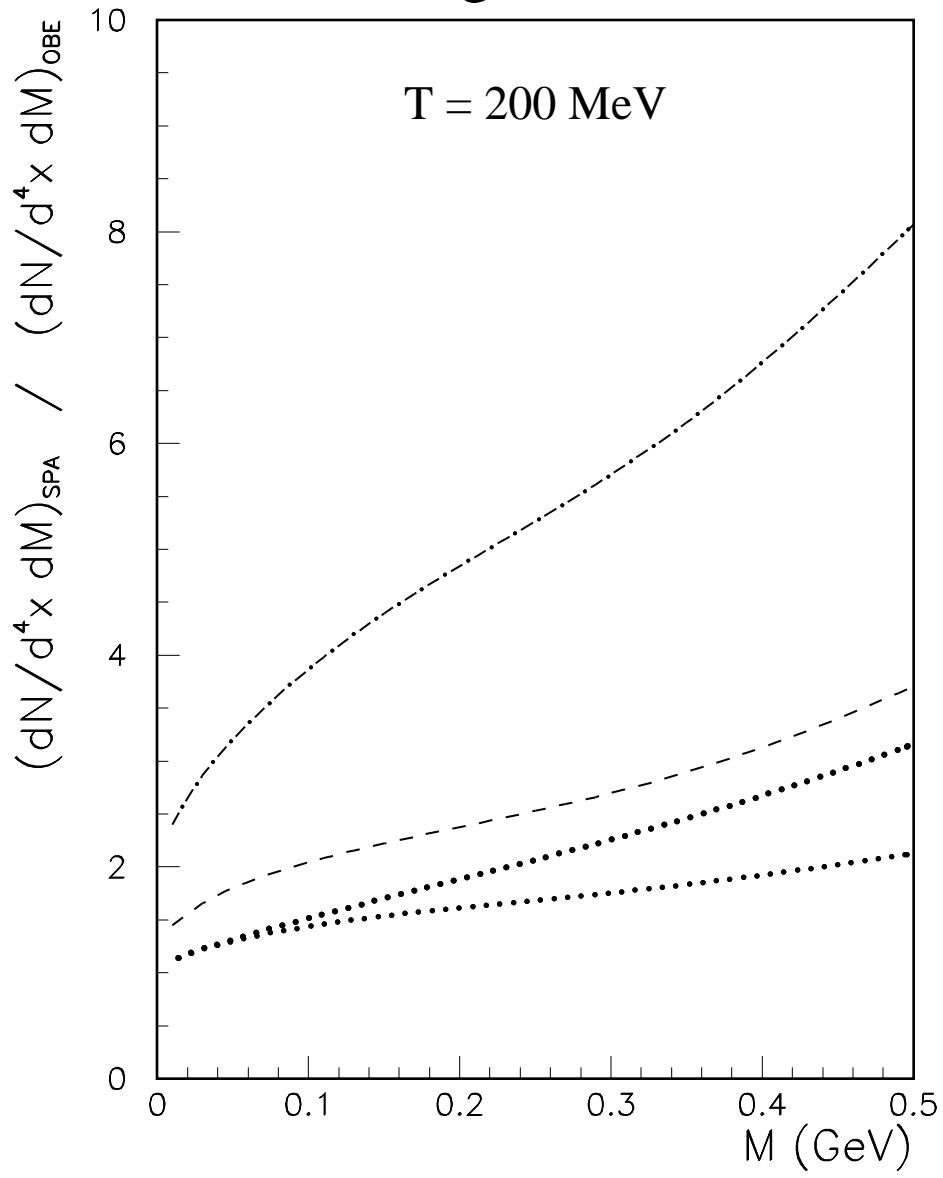


Figure 14

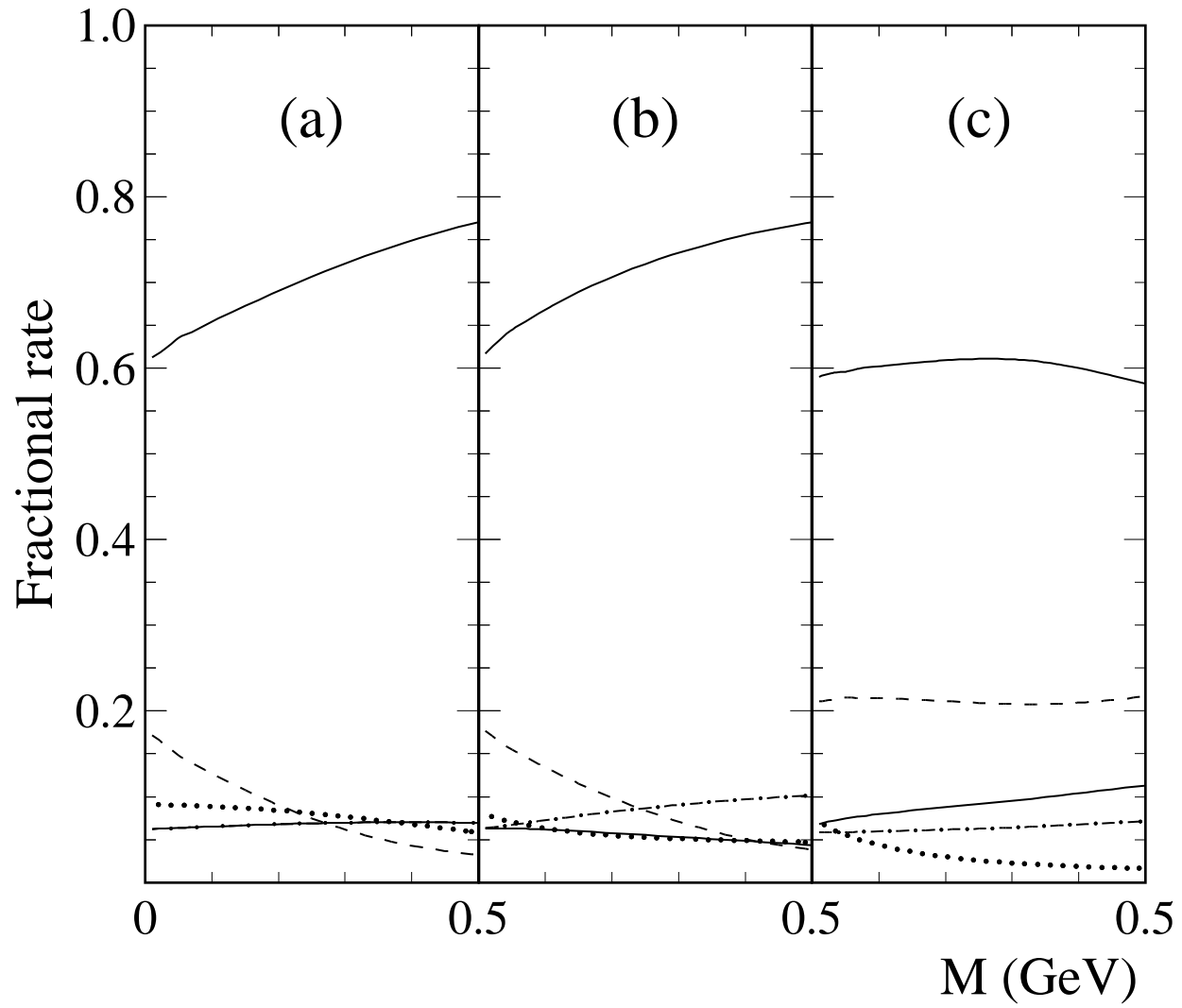


Figure 15

